

For the marked-up version of the manuscript, we use the following formatting definitions:

- Red strikethrough font shows a deletion
- Blue underlined font is an insertion

## Using Neural Network Ensembles to Separate Ocean Biogeochemical and Physical ~~Components~~ Drivers of Phytoplankton Biogeography in Earth System Models

Christopher Holder<sup>1</sup>, Anand Gnanadesikan<sup>1</sup>, Marie Aude-Pradal<sup>1</sup>

5 <sup>1</sup>Morton K. Blaustein Department of Earth and Planetary Sciences, Johns Hopkins University, Baltimore, MD, United States of America

Correspondence to: Christopher Holder (cholder2@jh.edu)

**Abstract.** Earth system models (ESMs) are useful tools for predicting and understanding past and future aspects of the climate system. However, the biological and physical parameters used in ESMs can have wide variations in their estimates. Even small changes in these parameters can yield unexpected results without a clear explanation of how a particular outcome was reached. The standard method for estimating ESM sensitivity is to compare spatiotemporal distributions of variables from different runs of a single ESM. However, a potential pitfall of this method is that ESM output could match observational patterns because of compensating errors. For example, if a model predicts overly weak upwelling and low nutrient concentrations, it ~~may~~might compensate for this by allowing phytoplankton to have a high sensitivity to nutrients. Recently, ~~it has been~~we demonstrated that neural network ensembles (NNEs) are capable of extracting relationships between predictor and target variables within ocean biogeochemical models. Being able to view the relationships between variables, along with spatiotemporal distributions, allows for a more mechanistically based examination of ESM outputs. Here, we investigated whether we could apply NNEs to help us determine why different ESMs produce different ~~results~~spatiotemporal distributions of phytoplankton biomass. We tested this using three cases. The first and second case ~~use~~used different runs of the same ESM, except ~~that~~ the physical circulations ~~differ~~differed between them in the first case while the biological equations ~~differ~~differed between them in the second. Our results ~~indicate~~indicated that the NNEs were capable of extracting the relationships between variables for different runs of a single ESM, allowing us to distinguish between differences due to changes in circulation (which do not change relationships) from changes in biogeochemical formulation (which do change relationships). In the third case, we applied NNEs to two different ESMs. The results of the third case highlighted the capability of NNEs to contrast the apparent relationships of different ESMs and some of the challenges it presents. Although applied specifically to the ocean components of an ESM, our study demonstrates that Earth System Modellers can use NNEs to separate the contributions of different components of ESMs. Specifically, this allows modellers to compare the apparent relationships across different ESMs and observational datasets.

30 **1 Introduction**

Earth system models (ESMs) are increasingly used to help us understand how anthropogenic greenhouse gas emissions will affect biological systems and how such changes will feed back on the climate system. Although these methods provide an avenue for examining processes on a global scale, their representations of biological and physical processes of the natural world are limited by imperfect knowledge and the inability to resolve these processes with current models which require ever increasingly higher computational costs for additional complexity and resolution. As a result, estimates of critical biological and physical parameters can vary quite substantially. For example, from tracer experiments in the North Atlantic subtropical gyre, diapycnal diffusivity was estimated between 0.1 to 0.5 cm<sup>2</sup> s<sup>-1</sup> (Ledwell et al., 1998), with similar values having been used in ESMs. Varying the diapycnal diffusivity within this range in ESMs has been shown to yield different results in the biogeochemical output (Oschlies, 2001; Duteil and Oschlies, 2011). Furthermore, ESMs do not agree about how to represent phytoplankton growth parameters, such as temperature dependence. In the nine ESMs compared in Laufkötter et al. (2015), the Q<sub>10</sub> value describing the sensitivity of growth rate to 10 degree increases in temperature ranged from 1.68 to 3, with some models varying the Q<sub>10</sub> values based on the size or type of phytoplankton.

45 The uncertainty associated with some ESM parameters can make it difficult to understand why different ESMs may yield different predictions for biological variables ranging from productivity to carbon uptake. Bopp et al. (2013) demonstrated that while CMIP5 models showed the same overall global trends under climate change for variables such as pH, sea surface temperature, O<sub>2</sub>, and primary productivity, there were ~~significant~~substantial cross-model differences in O<sub>2</sub> and primary productivity on regional scales.

Formatted: English (United Kingdom)

50 Traditional methods used to estimate the sensitivity of ESMs often compare the spatial distributions of biological and physical variables from different runs of a single ESM to each other or to observations. However, occasionally changes in one parameter improve the simulation of one variable while degrading the simulation of another (see for example, Bahl et al. (2019), their Table 2). Other times, errors in one variable are due to errors in another (i.e., getting a physical front in the wrong place may mean that the biomass has the wrong distribution).

55 The intent of ESMs is to get the correct spatial distribution both because the correct relationships between environmental predictors and target variables are being modelled and because the environmental predictors themselves are correctly modelled. However, it's difficult to know if the correct relationships are indeed being modelled. Thus, a method is needed in which we can evaluate whether different ESMs yield different projections because of fundamental differences in biogeochemical formulation, or whether such differences are primarily due to differences in physical circulations and climate sensitivities. Of the potential methods available, neural network ensembles (NNEs) are a strong candidate. NNEs are a machine learning (ML) technique which use the average of many individual neural networks (NNs) to predict the outcome of datasets. The objective of this paper is to investigate whether the application of NNEs and sensitivity analyses can provide useful information for determining the most substantial sources of differences in ESM outputs.

Formatted: Font: Not Italic

~~It was~~ We previously demonstrated that ~~neural-network-ensembles~~ (NNEs) were able to extract relationships between biological forcings and outputs within a simplified biogeochemical model (Holder and Gnanadesikan, ~~2021a~~2021). NNEs were able to outperform other ~~machine-learning~~ ML algorithms, such as random forests. More importantly, NNEs also had the benefits of being able to extrapolate outside the range of the training dataset and to provide a measure of their uncertainty in their predictions. ~~In~~ Holder and Gnanadesikan (~~2021a~~2021), ~~we~~ defined two types of relationships between environmental forcings and biological responses: intrinsic and apparent. *Intrinsic* relationships are those where the effect of one predictor variable on an outcome (target variable) can be examined, while maintaining other predictors at a constant level. An example of this would be ~~the results of a laboratory experiment~~ examining how ~~the growth rate of a particular species of~~ phytoplankton ~~react to~~ depends on different nutrient concentrations ~~in a nutrient-growth experiment~~, while all other factors remain constant. For ESMs, an example might be the Michaelis-Menten relationships ~~programmed into ESMs~~ that represent how phytoplankton interact with ~~nutrients~~ each nutrient. *Apparent* relationships are determined by how the intrinsic relationships interact across space and time, where individual variables are not controlled but may systematically co-vary. An example of this would be ~~the relationships that emerge in the output of ESMs, where the intrinsic relationships programmed into the ESM have interacted with one another across time and space and then had their outputs averaged into monthly-averaged fields. An example of this in the context of real-world environments would be~~ comparing satellite observations of phytoplankton distributions against monthly distributions of nutrients; where low phytoplankton concentrations may result both from low nutrients and high ~~light~~ irradiance in the summer in some locations, but also high nutrients and low ~~light~~ irradiance in the winter in other locations. As a result, the apparent relationships between nutrients and biomass would not resemble the intrinsic Michaelis-Menten curves coded in the ESM. A proof-of-concept application of NNEs coupled with sensitivity analyses at the end of Holder and Gnanadesikan (~~2021a~~2021) demonstrated the ability of NNEs to draw out the ~~co-limitations~~ co-limitations in a non-linear biogeochemical model and illustrated how these ~~co-limitations~~ co-limitations differed from the Michaelis-Menten curves programmed into the model.

~~The objective of~~ For this ~~paper is~~ study, we focus on marine phytoplankton physiology, but these approaches are also applicable to investigate whether the application of NNEs ~~other components of ESMs, including atmospheric and sensitivity analyses can provide useful information for determining differences in ESM outputs, terrestrial~~. In general, there are ~~three~~ two primary drivers that lead to differences in ~~the output of ESMs~~ how ESMs simulate phytoplankton biogeography: physical forcings ~~and~~ phytoplankton physiology ~~or combinations~~. Insofar as both of these ~~two~~ act to affect nutrient cycling they can also act in combination to produce indirect impacts. Before applying this method to outputs of multiple ESMs, we ~~chose to~~ investigate whether the method ~~worked~~ works well on different runs of a single ESM in which physical parameters ~~were~~ are changed to produce different circulations. It ~~was~~ is uncertain whether the NNEs ~~would be~~ are able to pick out the same apparent relationships of the same ESM when there ~~were~~ are differences between runs in the physical forcings and intrinsic biological equations (phytoplankton physiology). If different versions of an ESM, which have different circulations, still yield the same apparent relationships between ~~light~~ irradiance/nutrients and biomass, it would suggest that circulation changes do not produce new patterns of co-

105 limitation. It is worth noting that we are only stating this in the context of ESMs, as this may not necessarily be true in the real ocean. Furthermore, it would suggest that differences in the apparent relationships of *different* ESMs could be partitioned between those due to different physical circulations and those with different representations of biology. For example, if one uses the apparent relationships from model A to predict the biomass from model B given the environmental parameters from model B, any differences should be due to differences in the biological formulation.

110 To investigate the extent to which NNEs could characterize differences across ESMs, we ~~explored~~explore three cases:

1. We ~~examined~~examine an ESM in which biomass ~~was~~is by construction a function of nutrients and ~~light~~irradiance. Using three different runs of this ESM, we ~~maintained~~maintain identical intrinsic biological relationships, but ~~varied~~vary the physical parameters controlling the circulation across the different runs. The objective of the first case ~~was~~is to quantify the extent to which differences in physical circulation might affect the apparent relationships between predictor (~~light~~irradiance, nutrient, and temperature) and target (biomass) variables found by NNEs. If models with different circulations ~~produced~~produce differences in the apparent relationships, this would indicate that differences in circulation could push the biology into fundamentally new states- i.e., phytoplankton in one location experience new combinations of co-limitation or temporal variability (as described by Henson et al. (2021)). However, if the NNEs ~~found~~find the same apparent relationships between runs when the physical circulation ~~was~~is changing, this would indicate that the primary effect of changing the circulation ~~was~~is simply to change the times and locations where different combinations of ~~light~~irradiance and nutrients ~~were~~are found, rather than creating ~~fundamentally new states~~new patterns of co-limitation, i.e., phytoplankton are governed by the same dynamics/equations regardless of location.
- 125 2. We ~~used~~use the same ESM as that of Case 1, except we ~~maintained~~maintain similar physical circulations between runs and ~~changed~~change the intrinsic biological relationships- (this results in a small change in circulation because within our ESM the biological cycle affects physical circulation by changing the absorption of shortwave radiation). The objective of the second case ~~was~~is to quantify the ability of NNEs to detect differences in the apparent relationships when the intrinsic biological relationships between model runs ~~were~~are different and to document the size of those differences.
- 130 3. For the final case, we ~~looked~~look at two *different* ESMs that ~~had~~have different biogeochemical codes but ~~were~~are run within the same physical model giving them identical physical circulations. The first ESM ~~followed~~follows the framework of the ESMs in Cases 1 and 2, where biomass ~~was~~is a function of nutrients. The second ESM ~~allowed~~allows biomass to be advected and diffused, making biomass a function of nutrients, ~~light~~irradiance, and physical circulation. The objective of the third case ~~was~~is to apply the principles from Cases 1 and 2 to more standard ESMs, to quantify the extent to which physical circulation contributes to these apparent relationships, and to identify challenges in comparing the apparent relationships between ESMs.

## 2 Methods

### 2.1 Earth System Models – Biogeochemical Codes

In general, [ocean](#) biogeochemical components (BCs) of ESMs predict the evolution of phytoplankton biomass,  $B$ , using equations that have the general form

$$\frac{\partial B}{\partial t} + \vec{u} * \nabla B = \mu(N, \text{Light}, T)(N, I, T) * B - G(B, \dots) + \nabla * \vec{K} * \nabla B \quad (1)$$

where  $\vec{u}$  is the three-dimensional velocity field,  $\mu$  is the phytoplankton growth rate which is a function of nutrients  $N$ , [light irradiance](#)  $I$ , and temperature  $T$ ,  $G(B, \dots)$  represents the grazing loss rate, which may be a function of phytoplankton biomass and/or other variables such as temperature or zooplankton concentration, and  $\vec{K}$  is the three-dimensional mixing tensor. Changes in physical parameters (for example changing the values in  $\vec{K}$ ) would produce changes in transport of biomass. But the associated changes in circulation would also produce changes in other fields, such as  $N$ , [Light](#), and  $T$  (and thus in growth rate  $\mu$ ). Differences in the physical parameters between models will produce both direct differences, due to transport, and indirect differences, due to changes in growth and/or grazing. Additionally, insofar as the biology affects the absorption of shortwave radiation, it can produce differences in the circulation, [\(Sweeney et al., 2005\)](#), although for the simulations in this paper the differences are relatively small.

For this paper, we ~~chose to~~ focus on ~~biogeochemistry components (the ocean BCs)~~ run within two ESMs: Biogeochemistry with Light, Iron, Nutrients, and Gases (BLING) and Tracers of Phytoplankton with Allometric Zooplankton (TOPAZ). ~~In general terms~~ As described below, BLING ~~is~~ can be thought of as a simplified version of TOPAZ. For Cases 1 and 2, we ~~chose to~~ only use model runs within different versions of GFDL ESM2Mc, in which BLING is the BC, with the reasoning that if the NNEs ~~were~~ are unable to distinguish apparent relationships in the simpler BLING model, they would not be able to do so in the more complex TOPAZ model. In Case 3, we use versions of the GFDL ESM2M model in which BLING and TOPAZ are used as the BCs to compare apparent relationships found within the ESM.

### 2.2 Biogeochemistry with Light, Iron, Nutrients, and Gases (BLING)

BLING is a diagnostic biogeochemical model (Fig. 1) described in Galbraith et al. (2010), which was developed as a relatively [computationally](#) cheap biogeochemical code that could be run in high-resolution models. Only four explicit tracers are included in ~~within~~ the model: oxygen, dissolved organic phosphorus, phosphate, and iron (the last two corresponding to the nutrients (N) in Fig. 1). Phytoplankton are represented as two size classes: small and large (Biomass (B) in Fig. 1). Phytoplankton growth and grazing  $G(B, T)$  are modelled using the phytoplankton size-dependent loss equation developed by Dunne et al. (2005) represented as

$$\mu(N, \text{Light}, T)(N, I, T) * B \approx G(B, T) = \lambda \left( \frac{B}{P_*} \right)^\alpha B \quad (2)$$

where  $\lambda$  is a grazing rate,  $P_*$  is a biomass scaling for grazing, and  $\alpha$  is a grazing exponent. The grazing rate includes all losses due to grazing, viral lysis, temperature-dependent loss, and others. For the small phytoplankton size class  $\alpha$

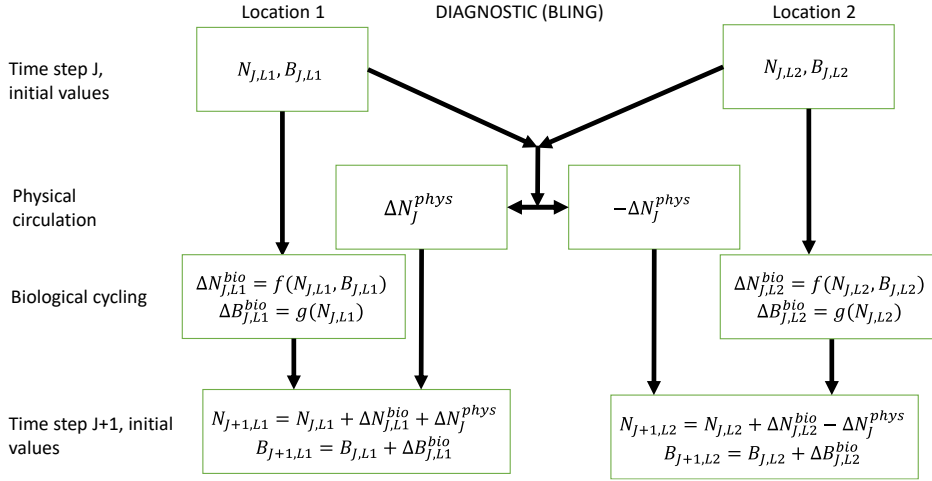


**Figure 1:** Conceptual diagram of how biogeochemical evolution is computed within an ESM using the BLING-BC. The letters and abbreviations represent: nutrients (N), phytoplankton biomass (B), the physical circulation component (phys), and the biological cycling component (bio). Each location has initial values for nutrients and biomass. These initial values are passed to the intrinsic biological relationships which then feed into the  $g$  function in the biological cycling box that are then used to calculate the changes in nutrients and biomass due to biological cycling. The initial nutrient concentrations between the two locations result in a change in nutrients from physical transport, which is equal in magnitude and opposite in sign between the two boxes (physical circulation component). When the physical circulation and biological cycling portions are coupled together, the nutrients and biomass for the next time step are calculated.

= 1 and for the large phytoplankton size class  $\alpha = 1/3$ . This means the large phytoplankton biomass is more sensitive to environmental conditions than the small phytoplankton biomass. The growth rate ( $\mu$ ) in Eq. (2) goes as

$$\begin{aligned} \mu &= \mu_o \cdot \exp(kT) \cdot \min\left(\frac{Fe}{K_{Fe} + Fe}, \frac{PO_4}{K_{PO_4} + PO_4}\right) \cdot \left(1 - \exp\left(-\frac{I \cdot r}{K_{Irr}}\right)\right) \cdot \mu \\ &= \mu_o \cdot \exp(kT) \cdot \left(1 - \exp\left(-\frac{I}{K_I}\right)\right) \cdot \min\left(\frac{Fe}{K_{Fe} + Fe}, \frac{PO_4}{K_{PO_4} + PO_4}\right) \end{aligned} \quad (3)$$

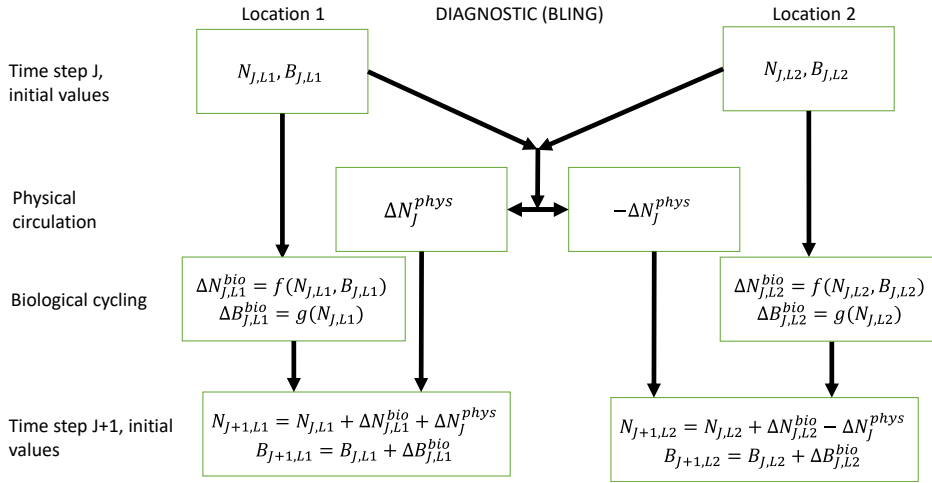


**Figure 1:** Conceptual diagram of how biogeochemical evolution is computed within an ESM using the BLING BC. The letters and abbreviations represent: nutrients (N), phytoplankton biomass (B), the physical circulation component (phys), and the biological cycling component (bio). Each location has initial values for nutrients and biomass. These initial values are passed to the intrinsic biological relationships which then feed into the g function in the biological cycling box that are then used to calculate the changes in nutrients and biomass due to biological cycling. The initial nutrient concentrations between the two locations result in a change in nutrients from physical transport, which is equal in magnitude and opposite in sign between the two boxes (physical circulation component). When the physical circulation and biological cycling portions are coupled together, the nutrients and biomass for the next time step are calculated.

where  $\mu$  is the growth rate,  $T$  is the temperature with constant  $k = 0.063^\circ\text{C}^{-1}$  following Eppley (1972),  $K_{Fe,PO_4}$  are the half-saturation constants, and  $I_{Fe}$ ,  $PO_4$ , and  $I_{irr}$  are the irradiances and the concentrations of dissolved iron, and phosphate, and irradiance, respectively.  $K_j$  is a function of the nutrient and temperature dependent growth rate, following Geider et al. (1997). The time averaged biomass then goes as

$$\bar{B} \approx \left(\frac{\mu}{\lambda}\right)^{\frac{1}{\alpha}} P, \quad (4)$$

175 Note that this means that given  $N$ ,  $I_{irr}$ , and  $T$  (all of which are still predicted by the circulation model), the apparent relationships between biomass, nutrients, and  $I_{irr}$  are potentially tightly coupled to the intrinsic relationships governing phytoplankton physiology that determine the growth rate.

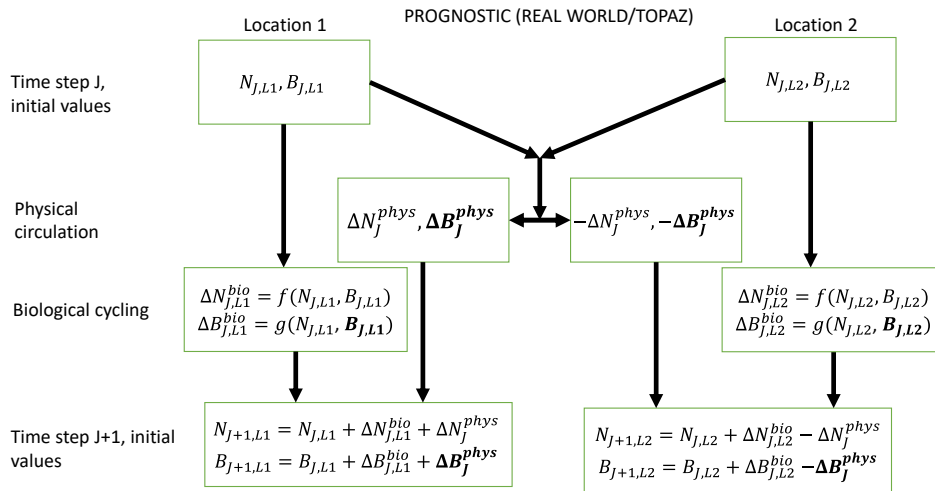


**Figure 2:** Conceptual diagram of how biogeochemical evolution is computed within an ESM using the prognostic TOPAZ-BC. The letters and abbreviations represent: nutrients (N), phytoplankton biomass (B), the physical circulation component (phys), and the biological cycling component (bio). This ESM differs from the one described in Fig. 1. In this prognostic model, the changes in biomass from the biological cycling component are a function of the nutrients and biomass, rather than nutrients alone. Additionally, a change in biomass due to physical circulation is added.



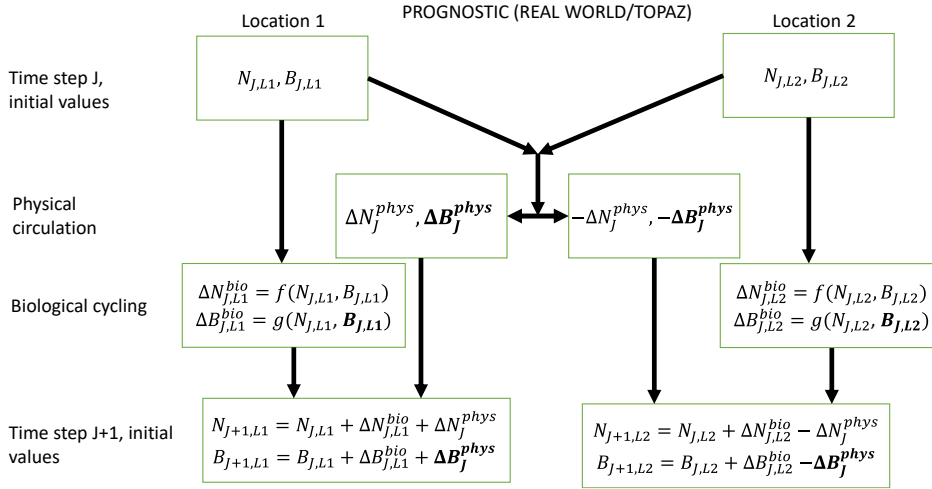


**Figure 2:** Conceptual diagram of how biogeochemical evolution is computed within an ESM using the prognostic TOPAZ BC. The letters and abbreviations represent: nutrients (N), phytoplankton biomass (B), the physical circulation component (phys), and the biological cycling component (bio). This ESM differs from the one described in Fig. 1. In this prognostic model, the changes in biomass from the biological cycling component are a function of the nutrients and biomass, rather than nutrients alone. Additionally, a change in biomass due to physical circulation is added.

### 2.3 Tracers of Phytoplankton with Allometric Zooplankton (TOPAZ)

180 TOPAZ is a prognostic biogeochemical model included in the Geophysical Fluid Dynamics Laboratory (GFDL) ESM2M (Dunne et al., 2013; Fig. 2). It includes a total of 30 tracers to model cycles such as nitrogen, phosphorus, iron, oxygen, carbon, and others (Nutrients (N) in Fig. 2). TOPAZ models three phytoplankton groups (small, large, and diazotrophic; Biomass (B) in Fig. 2) with **light irradiance** limitation based on the equations of Geider et al. (1997). Additionally, phytoplankton loss/grazing and particle export are modelled using the same size-dependent formulation as those used in Eq. (2), though without imposing the quasi-equilibrium assumption that leads to Eq. (4). TOPAZ differs from BLING in its number of tracers (and associated limitations) and the allowance for advection/diffusion of nutrients and biomass ( $\Delta B_j^{phys}$  in Fig. 2). This means that the loss rate of phytoplankton in TOPAZ is effectively a function of circulation as well the temperature and biomass-dependent grazing rate,  $\lambda \left( \frac{B}{B_c} \right)^\alpha$ . This will produce different biomasses in locations that have the same growth rates. Additionally, a key difference between BLING and 190 TOPAZ is that the latter includes denitrification and nitrogen fixation. This then means (as suggested by Tyrrell

(1999)) that the nitrogen is the proximate limiting nutrient, while phosphorus is the ultimate limiting nutrient; a distinction that is not made in BLING.

### 3 Case Descriptions

#### 3.1 Case 1 - Same ESM: Identical Biological Equations, Different Physical Circulations

195 The aim of Case 1 ~~was~~is to quantify the extent to which differences in physical circulations between model runs of the same ESM with identical intrinsic biological relationships ~~would~~could affect the apparent relationships found by NNEs. As stated in Section 2.1, we ~~chose to~~ compare versions of GFDL ESM2Mc in which BLING is configured identically so we can be certain the differences are solely due to circulation changing the environmental conditions, and not the phytoplankton loss rates. Within GFDL ESM2Mc, the nominal resolution is 3 degrees longitudinally and  
200 2 degrees latitudinally, while the vertical resolution has 28 levels. Model runs are initialized with observations and spun up for 1900 years. The final 100 years are used to generate a monthly climatology.

We ~~chose to~~ use three configurations of GFDL ESM2Mc. The three model runs ~~consisted~~consist of: a standard historical pre-industrial model spin-up (BLING – PI Control), a similar case to the first but where the carbon dioxide concentration ~~was~~is four times higher (BLING – 4x CO<sub>2</sub>), and a case similar to the historical spin-up except that the horizontal mixing parameter ~~was~~is three times higher (BLING – 3x Mixing). These model runs are described in greater detail in Gnanadesikan et al. (2013), Pradal and Gnanadesikan (2014), and Bahl et al. (2020). With the standard historical model essentially serving as a form of a “control,” the two remaining cases ~~allowed~~allow us to examine if changes in the physical circulation ~~would~~could result in changes to the apparent relationships.

210 The predictor variables for each model run ~~were~~are macronutrient (~~ex-c.g.~~, phosphate), micronutrient (~~ex-c.g.~~, dissolved iron), irradiance, and temperature. The target variables ~~were~~are small phytoplankton biomass and large phytoplankton biomass. One NNE ~~was~~is trained for each target variable of each model run for a total of six NNEs in Case 1 (three model runs and two target variables in each run). Details of the NNE training and the construction of  
215 the individual NNs making up each NNE can be found in Section ~~2-3.4~~.

#### 3.2 Case 2 - Same ESM: Different Diagnostic Biological Equations, Near-Identical Physical Circulations

The purpose of Case 2 ~~was~~is to quantify the differences found by NNEs between the apparent relationships of model runs from the same ESM when the biological equations differ between runs, but the physical circulations are nearly identical.

220 As in Case 1, we ~~again chose to~~ use different configurations of ESM2Mc, but this time we keep the physical parameterizations constant but change constants within the BLING BC. We ~~used~~use two model runs: the standard historical pre-industrial model spin-up used in Case 1 (BLING – PI Control) and one with similar distributions to PI Control but different half-saturation coefficients ( $K_{Fe}$  and  $K_{PO4}$  in Eq. (3)) for small and large phytoplankton (BLING

225 – LgSm). Changing the half-saturation coefficients, which directly affects phytoplankton growth, is analogous to  
changing the biological equations. Relative to the PI Control, the half-saturation coefficients in LgSm ~~were~~are  
decreased by  $\sqrt{3}$  for small phytoplankton and increased by  $\sqrt{3}$  for large phytoplankton. While these changes produce  
~~small~~ differences in circulation and SST ( ~~$R^2 = 0.9949$  for SST between the two model runs~~) via changing the  
absorption of shortwave radiation, these differences are small. ( $R^2 = 0.9949$  for SST between the two model runs).  
230 The primary impact of these changes ~~affects~~is to affect the distribution of nutrients, as increasing the half-saturation  
coefficients for large phytoplankton makes it harder for these phytoplankton to grow and efficiently export nutrients.

The predictor variables for the model runs of Case 2 ~~were~~are the same as those in Case 1 (macronutrient, micronutrient,  
irradiance, and temperature). Likewise, the target variables ~~were~~are also the same as those in Case 1 (small and large  
235 phytoplankton biomass). A total of four NNEs ~~were~~are trained for Case 2 (two model runs and two target variables).

### 3.3 Case 3 - Different ESMs: Prognostic vs. Diagnostic Biological Equations, Identical Physical Circulations

For Case 3, the goal ~~was~~is to examine whether the results from a diagnostic BC from Cases 1 and 2 still ~~held~~hold  
when a prognostic BC ~~was~~is used. Our goal ~~was~~is to examine any differences in apparent relationships, along with  
identifying challenges when comparing apparent relationships across more realistic ESMs. In this experiment, the BCs  
240 ~~were~~are governed by different biological equations; but ~~were~~are run within the same physical model so that the  
temperatures and ~~light~~irradiance seen by the two BC codes ~~were~~are identical.

One of our model simulations uses a version of BLING as the BC, while the other uses TOPAZ. For the BLING model  
run, the iron concentrations ~~were~~are fixed at their climatological values since this formulation was previously used to  
245 develop a model for very high-resolution studies (miniBLING). We ~~chose~~use this pair of simulations ~~as~~since the  
miniBLING code ~~was~~is run in an identical physical circulation to the TOPAZ model run and so the ~~light~~irradiance  
and temperature experienced by the two model ecosystems are identical. ~~As~~The ESM2M uses a 1 degree  
latitude/longitude resolution with 50 vertical layers and the model is spun up for 2400 years. These simulations are  
described in more detail in Galbraith et al. (2015), the output is from the which shows that BLING and miniBLING  
250 yield essentially identical predictions for carbon uptake and ocean ~~component of ESM2M forced with historical~~  
~~atmospheric forcing which we denote as ESM2Mo-~~ deoxygenation under increased CO<sub>2</sub>.

The predictor variables for Case 3 ~~were~~are limited to variables that ~~were~~are present in both ESMs: macronutrient,  
micronutrient, and irradiance. The target variable ~~was~~is total biomass. The biomass ~~was~~is not split into small and large  
255 phytoplankton biomass because the miniBLING output only ~~contained~~contains total biomass. For consistency, the  
small and large phytoplankton biomass values in TOPAZ ~~were~~are combined to give total biomass. Two NNEs ~~were~~are  
trained for Case 3 (two ESM runs and one target variable).

### 3.4 Neural Network Ensembles (NNEs)

260 ~~Neural network ensembles (NNEs)~~ are an ensemble ~~machine learning (ML)~~ method. NNEs are comprised of a collection of individual ~~neural networks (NNs)~~ where the predictions of each NN are averaged into a single prediction. This ensemble approach has been shown to outperform individual NNs and reduce the generalization error within a dataset (Hansen and Salamon, 1990) by turning individual “weak learners” into a single “strong learner.” Individual ~~neural networks (NNs)~~ can fit a non-linear function to a dataset without assuming any prior knowledge of the system. For a more thorough discussion of NNs, please refer to Schmidhuber (2015). The basic structure of the NN approach 265 that we use here is described in Appendix 1 of Scardi (1996).

We ~~chose to~~ use NNEs for several reasons:

1. The ensemble approach of NNEs allows us to view the uncertainty in any given prediction based on the individual predictions of each NN.
- 270 2. NNEs possess some capability of extrapolating outside the range of the data on which they are trained. ([Holder and Gnanadesikan, 2021](#)).
3. As recently shown in Holder and Gnanadesikan (~~2021a~~[2021](#)), NNEs were able to more closely reproduce the underlying intrinsic relationships compared to ~~RFs~~[random forests](#), mainly because of their ability to extrapolate.

275 The structure of the individual NNs ~~was~~[is](#) consistent between the three cases with each NN containing 25 ~~hidden~~ nodes in the hidden layer with a hyperbolic tangent sigmoid activation function and 1 node in the output layer with a linear activation function. [We demonstrated in previous work that the NNE predictions were not greatly improved with the addition of a second hidden layer or with hidden layer node quantities greater than 25 \(Holder and Gnanadesikan, 2021\). Additionally, the activation function of the hidden layer nodes did not see a substantial increase in performance either as long as a non-linear function was used \(Holder and Gnanadesikan, 2021\). The ~~only~~ settings specified here allow for reasonable training times while maintaining high performance metrics relative to the other formulations tested in our previous work \(Holder and Gnanadesikan, 2021\). For more detailed information, see Appendix B2 in Holder and Gnanadesikan \(2021\).](#)

285 [The](#) difference between each case ~~was~~[is](#) in the number of input nodes: Cases 1 and 2 each ~~contained~~[contain](#) four input nodes (one for each predictor) and Case 3 ~~contained~~[has](#) three input nodes. [The predicted concentration of each target variable \(second column of Table 1\) in individual NNs can be thought of as a function of the respective predictors \(first column of Table 1\).](#) For example, one NN of the NNE for the small phytoplankton biomass target variable in 290 Case 1 would have the following structure:

1. The four predictor variables for Case 1 (first column of Table 1) correspond to the four nodes in the input layer of the NN.
2. Each of the four input nodes is connected by weights to each of the 25 nodes in the hidden layer. Additionally, a bias term is connected to each of the hidden nodes.

**Table 1:** Summary of each case which includes information on the predictor variables, the target variables, the ESMs, the model runs, the biological specifications, and the physical circulation specifications.

Case #	Predictor Variables	Target Variables	Biogeochemical Component	Model Runs	Biological Specifications	Physics/Circulation Specifications
1	Macronutrient (mol kg <sup>-1</sup> ); Micronutrient (mol kg <sup>-1</sup> ); Irradiance (W m <sup>-2</sup> ); Temperature (°C)	Small Phytoplankton Biomass (mol P kg <sup>-1</sup> ); Large Phytoplankton Biomass (mol P kg <sup>-1</sup> )	BLING	PI Control; 4xCO <sub>2</sub> ; 3x Mixing	Identical diagnostic BC across model runs	Predicted by different versions of ESM2Mc produced by significant changes in physical parameters
2	Macronutrient (mol kg <sup>-1</sup> ); Micronutrient (mol kg <sup>-1</sup> ); Irradiance (W m <sup>-2</sup> ); Temperature (°C)	Small Phytoplankton Biomass (mol P kg <sup>-1</sup> ); Large Phytoplankton Biomass (mol P kg <sup>-1</sup> )	BLING	PI Control; LgSm	Different diagnostic BC across model runs	Nearly identical circulations produced by ESM2Mc
3	Macronutrient (mol kg <sup>-1</sup> ); Micronutrient (mol kg <sup>-1</sup> ); Irradiance (W m <sup>-2</sup> )	Total Phytoplankton Biomass (mol P kg <sup>-1</sup> )	miniBLING and TOPAZ	One model run from miniBLING; one model run from TOPAZ	Simple diagnostic vs complex pronostic BC	Identical physical circulations produced by ocean component of ESM2M

295 3. Each of the nodes in the hidden layer is connected by weights to the single node in the output layer, which, for  
this instance, would correspond to the target variable of small phytoplankton biomass. As with the hidden layer,  
a bias term is connected to the single output node.

The training of each NN ~~was~~is carried out using the “feedforwardnet” function in MATLAB 2019b (MATLAB, 2019).  
300 For each trained NN, the “feedforwardnet” function is provided the training dataset, which it then automatically  
separates into training, validation, and testing subsets, with 70% of the observations from the training dataset going  
to the training subset, 15% to the validation subset, and 15% to the testing subset. The training ~~was stopped~~stops when  
the error between the predictions and observations ~~increased~~increases for six consecutive epochs.

305 Separate NNEs ~~were~~are trained for each response variable in each model run, which ~~equated~~equates to six NNEs (2  
target variables, 3 simulations) in Case 1, four NNEs in Case 2, and two NNEs in Case 3. For consistency, the same  
framework and settings ~~were~~are used for the construction of the NNEs with each one consisting of 25 individuals  
NNs.

~~It was demonstrated in Holder and Gnanadesikan (2021a) that the predictions produced by this approach were  
insensitive to the particular configuration of the NNEs. They tested various conditions that could affect the NNE  
performance including activation functions of the hidden layer nodes, number of hidden layers, and number of nodes  
in the hidden layer. The settings specified here allowed for reasonable training times while maintaining high  
performance metrics. For more detailed information, see Appendix B2 in Holder and Gnanadesikan (2021a).~~

315

Each variable [was is](#) also scaled between -1 and 1 relative to each variable's maximum and minimum

$$V_S = \frac{\max_S - \min_S}{\max_U - \min_U} (V_U - \min_U) + \min_S \quad (5)$$

Where V is the value of a variable being scaled, S (subscript) is the scaled value, and U (subscript) is the unscaled value. This scaling puts the predictor values in the same range, so more weight is not given to variables with larger ranges. Additionally, this step decreases the training time of the NNs so that no values are too close to the limits of the hyperbolic tangent sigmoid activation function. The variables and predictions [were are](#) then scaled back to their original values for analysis and presentation of the results (Eq. (6)). The letter representations in Eq. (6) are the same as those in Eq. (5).

$$V_U = \frac{\max_U - \min_U}{\max_S - \min_S} (V_S - \min_S) + \min_U \quad (6)$$

When using ML, it is possible to produce overly complex relationships that “overfit” the data. This provides a good match for the data on which an ML model is trained but leads to poor predictions when new data is presented to the model. This can be avoided by splitting a dataset into training and testing subsets. For this manuscript, this means each NNE [was is](#) trained using only the observations in the training subset and tested on the observations from the testing subset. The data from each model run [was is](#) randomly split into training and testing subsets with 60% of the observations from a dataset going to the training subset and the other 40% going to the testing subset. The observations set aside in the testing subset [were are](#) ones that the NNEs never [saw see](#) during their training phase. This provides a way to evaluate each trained NNE and its generalizability. If performance metrics of a trained NNE are similar between the training and testing subsets, it suggests that the variance of the dataset is well captured in the training phase and the NNE is generalizable to the entire dataset.

To assess the performance of each NNE, we [ealeulated calculate](#) the [standard](#)  $R^2$  values and root mean squared error (RMSE) by comparing the [monthly biomass](#) predictions from each NNE to the [actual“true” monthly biomass](#) values [of the model runs](#) within the respective training and testing subsets.

**Table 1: Summary of each case which includes information on the predictor variables, the target variables, the ESMs, the model runs, the biological specifications, and the physical circulation specifications.**

Case #	Predictor Variables	Target Variables	Biogeochemical Component	Model Runs	Biological Specifications	Physics/Circulation Specifications
1	Macronutrient (mol kg <sup>-1</sup> ); Mikronutrient (mol kg <sup>-1</sup> ); Irradiance (W m <sup>-2</sup> ); Temperature (°C)	Small Phytoplankton Biomass (mol kg <sup>-1</sup> ); Large Phytoplankton Biomass (mol kg <sup>-1</sup> )	BLING	PI Control; 4xCO <sub>2</sub> ; 3x Mixing	Identical diagnostic BC across model runs	Predicted by different versions of ESM2Mc produced by significant changes in physical parameters
2	Macronutrient (mol kg <sup>-1</sup> ); Mikronutrient (mol kg <sup>-1</sup> ); Irradiance (W m <sup>-2</sup> ); Temperature (°C)	Small Phytoplankton Biomass (mol kg <sup>-1</sup> ); Large Phytoplankton Biomass (mol kg <sup>-1</sup> )	BLING	PI Control; LgSm	Different diagnostic BC across model runs	Nearly identical circulations produced by ESM2Mc
3	Macronutrient (mol kg <sup>-1</sup> ); Mikronutrient (mol kg <sup>-1</sup> ); Irradiance (W m <sup>-2</sup> )	Total Phytoplankton Biomass (mol kg <sup>-1</sup> )	miniBLING and TOPAZ	One model run from miniBLING; one model run from TOPAZ	Simple diagnostic vs complex prognostic BC	Identical physical circulations produced by ocean component of ESM2M

The NNEs in each case and matching size class ~~were~~ also asked to make predictions on the testing subsets of the other model runs. For example, in Case 1 the NNE trained on the small phytoplankton of PI Control ~~was~~ asked to make predictions for small phytoplankton of 4xCO<sub>2</sub> using the values of the predictors from the testing subset of the 4xCO<sub>2</sub> model run. These results ~~were~~ then compared to the actual values of the target variable to calculate the RMSE. This RMSE ~~was~~ then used to calculate the percent increase/decrease in error when compared against the RMSE calculated from a point-by-point comparison of each model run against the others. The purpose of this ~~was~~ to provide another metric for testing if the NNEs ~~had found~~ common apparent relationships across model runs. If an NNE trained on one model run ~~was~~ able to ~~accurately~~ predict the outcomes of the other model runs ~~leading with errors that are similar in magnitude to a reduction in the RMSE~~ NNEs that were trained on those runs, it would suggest that the ~~NNE had found~~ NNEs are finding similar apparent relationships between the model runs. On the other hand, if it ~~showed~~ shows an increase in RMSE, it ~~would suggest~~ suggests that the apparent relationships between the model runs ~~were~~ are different in biologically important ways.

To view the apparent relationships found by the NNEs, we ~~conducted~~ conduct sensitivity analyses in which we ~~presented~~ present each NNE with a unique set of values for the predictors. Compared to spatiotemporal distributions and time series, sensitivity analyses allow for the visualization of relationships between predictor and target variables.

In each sensitivity analysis, one predictor ~~was~~ varied across its minimum and maximum range, while the other variables ~~were~~ held at a specified value, such as each variable's 25<sup>th</sup> percentile. This ~~was~~ repeated for the 50<sup>th</sup> and 75<sup>th</sup> percentile values of each variable as well. This ~~allowed~~ allows us to visualize how the biomass predictions ~~changed~~ change across one variable's range when the other variables ~~were~~ are held at a specified value. An example of

360 this ~~would be~~ varying the macronutrient concentration while holding the micronutrient, irradiance, and temperature variables at their 25<sup>th</sup> or 75<sup>th</sup> percentile values. This ~~allowed~~ allows us to see how the macronutrient concentration ~~affected~~ affects biomass when other nutrients ~~were~~ are low or high, respectively.

## 4 Results and Discussion

### 4.1 Case 1 – Same ESM: Identical Biological Equations, Different Physical Circulations

365 In Case 1, our objective ~~was~~ is to quantify the extent to which differences in physical circulation might affect the apparent relationships found by NNEs when the intrinsic biological relationships ~~remained~~ remain the same between the model runs and the physical circulation parameters ~~differed~~ differ. It ~~was~~ is uncertain whether changing the circulation would ~~push the biology into fundamentally~~ lead to new ~~states~~ patterns of co-limitation (i.e., different apparent relationships) or whether the physical circulation would simply act to change the location of where combinations of ~~high~~ irradiance and nutrients ~~were~~ are found (~~ie. i.e.~~ same apparent relationships).

370 Our results support the latter ~~case, in~~ outcome, that the locations of particular environments ~~were~~ are simply being shuffled around. The sensitivity analysis ~~showed~~ shows that each NNE ~~found~~ finds similar apparent relationships between biomass and each of the predictors for the respective size classes, insofar as each line ~~fell~~ falls within the standard deviation of the others (Fig. 3 and 4). For example, the standard deviation (gray region) around the predicted apparent relationships for the large phytoplankton (dashed lines) all overlap one another (Fig. 3). The same ~~can be~~ is seen for the predicted apparent relationships for the small phytoplankton (Fig. 4). Additionally, we ~~were~~ are confident in the apparent relationships since each NNE ~~acquired~~ acquires high performance metrics in both the training and testing subsets (highest RMSE =  $3.11 \times 10^{-9}$  mol ~~P~~ kg<sup>-1</sup>; Table 2) relative to the mean value of the total biomass ( $1.24 \times 10^{-8}$  mol ~~P~~ kg<sup>-1</sup>).



**Table 2:** The performance metrics for the training and testing subsets for the trained NNEs from each case separated into their respective size classes and ESM/model runs.

Case #	Phytoplankton Size	ESM/Model Run/BC	Training Data		Testing Data	
			R-squared	RMSE	R-squared	RMSE
Case 1	Small Phytoplankton	ESM2Mc / PI Control / BLING	0.9912	$6.24 \times 10^{-10}$	0.9908	$6.35 \times 10^{-10}$
		ESM2Mc / 4x CO <sub>2</sub> / BLING	0.9906	$6.18 \times 10^{-10}$	0.9903	$6.26 \times 10^{-10}$
		ESM2Mc / 3x Mixing / BLING	0.9912	$6.22 \times 10^{-10}$	0.9906	$6.35 \times 10^{-10}$
	Large Phytoplankton	ESM2Mc / PI Control / BLING	0.9790	$3.00 \times 10^{-9}$	0.9771	$3.11 \times 10^{-9}$
		ESM2Mc / 4x CO <sub>2</sub> / BLING	0.9749	$2.74 \times 10^{-9}$	0.9740	$2.77 \times 10^{-9}$
		ESM2Mc / 3x Mixing / BLING	0.9804	$3.00 \times 10^{-9}$	0.9778	$3.11 \times 10^{-9}$
Case 2	Small Phytoplankton	ESM2Mc / PI Control / BLING	0.9912	$6.24 \times 10^{-10}$	0.9908	$6.35 \times 10^{-10}$
		ESM2Mc / PI Control / BLING-LgSm	0.9762	$1.00 \times 10^{-9}$	0.9761	$1.00 \times 10^{-9}$
	Large Phytoplankton	ESM2Mc / PI Control / BLING	0.9790	$3.00 \times 10^{-9}$	0.9771	$3.11 \times 10^{-9}$
		ESM2Mc / PI Control / BLING-LgSm	0.9862	$2.34 \times 10^{-9}$	0.9855	$2.38 \times 10^{-9}$
Case 3	Total Phytoplankton	ESM2Mo / Historical / miniBLING	0.9511	$8.97 \times 10^{-9}$	0.9507	$9.11 \times 10^{-9}$
		ESM2Mo / Historical / TOPAZ	0.5893	$8.97 \times 10^{-9}$	0.5867	$8.99 \times 10^{-9}$

380

This result can be better understood by considering the conceptual diagram of how the diagnostic BC BLING works within an ESM (Fig. 1). For each time step, nutrients are calculated as a function of three terms: the initial nutrients, the change in nutrients from biology, and the change in nutrients from physical circulation. In contrast, the biomass is only a function of two terms: the initial biomass values and the change in biomass due to biological cycling. Thus, biomass is not directly affected by changes in the physical circulation. Additionally, this means that when given information on the biological predictors, but not the physical parameters, the NNEs ~~were able to back out the apparent relationships quite well~~ are able to back out the apparent relationships quite well. Although it would seem obvious from Fig. 1 that the biomass is not directly affected by changes in the physical circulation, we were unsure whether indirect impacts of such changes (changing patterns of co-limitation or temporal variability) would affect the results.

385

390

Our results indicate that such indirect effects were absent or, at most, minor.

**Table 2: The performance metrics for the training and testing subsets for the trained NNEs from each case separated into their respective size classes and ESM/model runs.**

Case #	Phytoplankton Size	ESM/Model Run/BC	Training Data		Testing Data	
			R-squared	RMSE	R-squared	RMSE
Case 1	Small Phytoplankton	ESM2Mc / PI Control / BLING	0.9912	$6.24 \times 10^{-10}$	0.9908	$6.35 \times 10^{-10}$
		ESM2Mc / 4x CO <sub>2</sub> / BLING	0.9906	$6.18 \times 10^{-10}$	0.9903	$6.26 \times 10^{-10}$
		ESM2Mc / 3x Mixing / BLING	0.9912	$6.22 \times 10^{-10}$	0.9906	$6.35 \times 10^{-10}$
	Large Phytoplankton	ESM2Mc / PI Control / BLING	0.9790	$3.00 \times 10^{-9}$	0.9771	$3.11 \times 10^{-9}$
		ESM2Mc / 4x CO <sub>2</sub> / BLING	0.9749	$2.74 \times 10^{-9}$	0.9740	$2.77 \times 10^{-9}$
		ESM2Mc / 3x Mixing / BLING	0.9804	$3.00 \times 10^{-9}$	0.9778	$3.11 \times 10^{-9}$
Case 2	Small Phytoplankton	ESM2Mc / PI Control / BLING	0.9912	$6.24 \times 10^{-10}$	0.9908	$6.35 \times 10^{-10}$
		ESM2Mc / PI Control / BLING-LgSm	0.9762	$1.00 \times 10^{-9}$	0.9761	$1.00 \times 10^{-9}$
	Large Phytoplankton	ESM2Mc / PI Control / BLING	0.9790	$3.00 \times 10^{-9}$	0.9771	$3.11 \times 10^{-9}$
		ESM2Mc / PI Control / BLING-LgSm	0.9862	$2.34 \times 10^{-9}$	0.9855	$2.38 \times 10^{-9}$
Case 3	Total Phytoplankton	ESM2Mo / Historical / miniBLING	0.9511	$8.97 \times 10^{-9}$	0.9507	$9.11 \times 10^{-9}$
		ESM2Mo / Historical / TOPAZ	0.5893	$8.97 \times 10^{-9}$	0.5867	$8.99 \times 10^{-9}$

That similar apparent relationships ~~were~~ found between the model runs ~~was~~ is further supported when we ~~tasked~~ task each trained NNE with making predictions on the testing subsets of the other model runs for the same size class. For example, the NNE trained on the PI Control for small phytoplankton ~~was~~ can be tasked with making predictions for the small phytoplankton biomass of 4xCO<sub>2</sub> and 3xMixing using the predictor values from their testing subsets. This test ~~allowed~~ allows for the evaluation of the robustness of the relationships that each NNE ~~found~~ finds. If the NNEs ~~were~~ are finding different relationships between the model runs, the NNE from one model run ~~would~~ will likely perform poorly when predicting ~~on~~ the other model runs. Our results show that the NNEs ~~performed~~ perform well when applied to the other model runs (highest RMSE =  $3.74 \times 10^{-9}$  mol P kg<sup>-1</sup>; Table 3) relative to the average value of total biomass

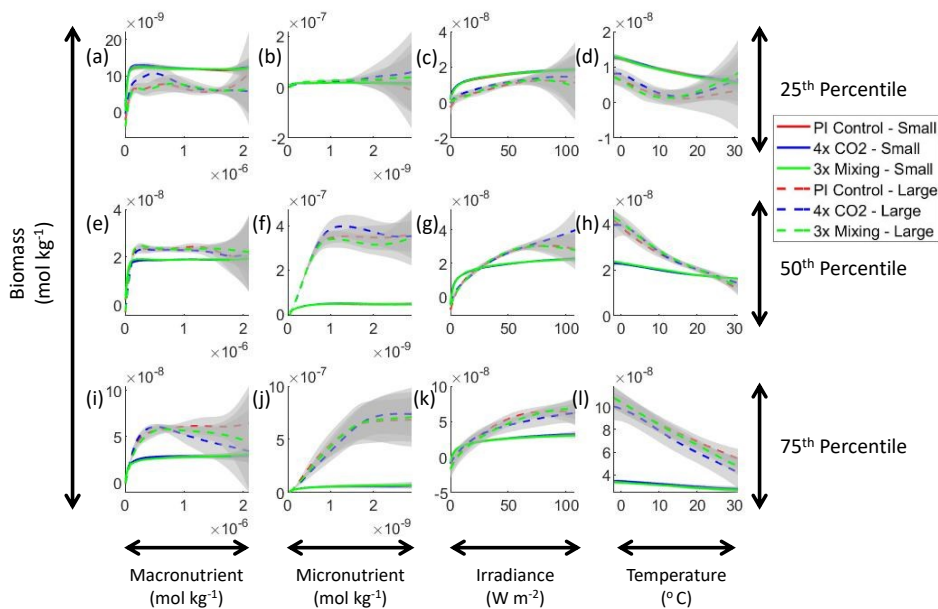


**Figure 3:** Sensitivity analysis plots for the small and large phytoplankton of Case 1. Each line is the prediction for the NNE specific to each model run and the color of each line represents the model run (PI Control—Red; 4xCO<sub>2</sub>—Blue; 3xMixing—Green). The solid lines correspond to the small phytoplankton and the dashed lines to the large phytoplankton. The gray region around each line shows one standard deviation in the predictions of the individual NNs that make up each NNE (ex. The gray region around the solid red curves shows the standard deviation in the predictions of the 25 NNs that make up that particular NNE). The rows correspond to the percentile value at which the other predictor variables were held constant (ex. Box (a) varies the macronutrient across its min-max range and holds the micronutrient, irradiance, and temperature at their respective 25<sup>th</sup> percentile values). Columns show the x-axis variables as they vary between their min-max range. The y-axis in all subplots is the biomass concentration. Note that the biomass scale changes with each subplot.

400 (1.24x10<sup>-8</sup> mol P kg<sup>-1</sup>). Given that these values are close to the performance metrics of their original datasets (Table 2 vs Table 3), it seems logical to say that this **was** because they **were** finding the same relationships.

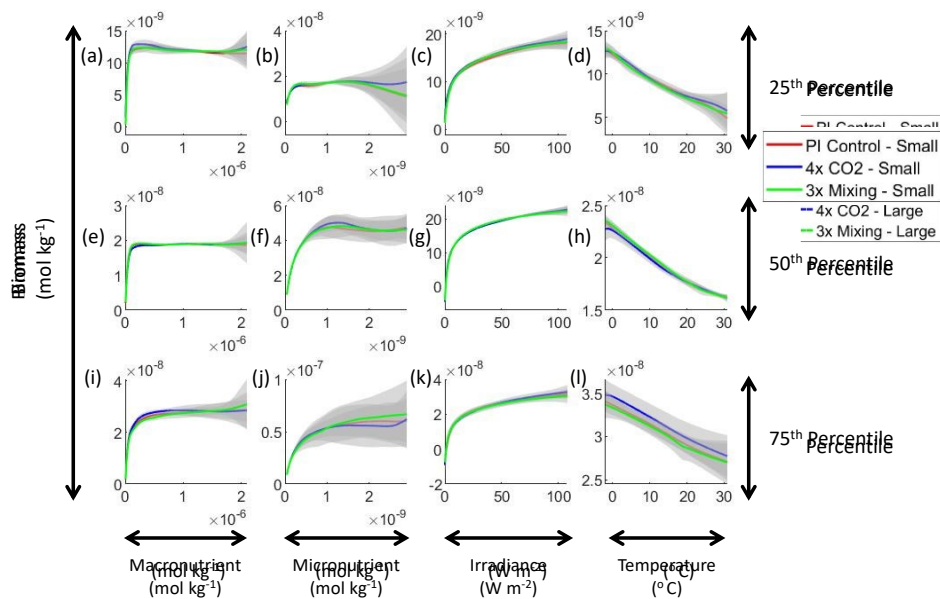


**Figure 3:** Sensitivity analysis plots for the small and large phytoplankton of Case 1. Each line is the prediction for the NNE specific to each model run and the color of each line represents the model run (PI Control—Red; 4xCO<sub>2</sub>—Blue; 3xMixing—Green). The gray region around each line shows one standard deviation in the predictions of the individual NNs that make up each NNE (ex. The gray region around the solid red curves shows the standard deviation in the predictions of the 25 NNs that make up that particular NNE). The rows correspond to the percentile value at which the other predictor variables were held constant (ex. Box (a) varies the macronutrient across its min-max range and holds the micronutrient, irradiance, and temperature at their respective 25th percentile values). Columns show the x-axis variables as they vary between their min-max range. The y-axis in all subplots is the biomass concentration. Note that the biomass scale changes with each subplot.

Additionally, using the NNEs to predict the other runs **led leads** to decreases in error relative to the error from comparing each run against the others. For example, the initial point-by-point comparison of 4xCO<sub>2</sub> and PI Control for small phytoplankton (Fig. 5 d) **showed shows** an RMSE of  $3.06 \times 10^{-9}$  mol P kg<sup>-1</sup>, while using the NNEs from each model run to predict the other saw the RMSE go down with a reduction in error of about 76% (Table 3). This reduction of error **was is** consistent across the other model runs and size classes with error reductions varying from 54-79%

**Table 3:** The performance metrics for the NNEs being used to predict the outcome of the other model runs for the same size class of Case 1. In the top half of the table, the R-squared and RMSE are listed. The values in parentheses are the values from comparing the respective cases against one another (these are the same values listed in the respective scatter plots of Fig. 5 and 6). The values outside the parentheses are the values from using the trained NNE of the model listed in the row to predict the outcome of the model run in the column (ex. The NNE trained on 4xCO<sub>2</sub> was used to predict the PI Control outcome using the predictor values of PI Control. These values were compared against the actual values of the PI Control to compute the RMSE of  $7.15 \times 10^{-10}$ ). In the bottom half of the table is the percent decrease in RMSE from the number listed inside the parentheses to the RMSE outside the parentheses.

				Case being predicted					
				Small Phytoplankton			Large Phytoplankton		
				PI Control	4x CO <sub>2</sub>	3x Mixing	PI Control	4x CO <sub>2</sub>	3x Mixing
<b>R-squared</b>	NNE being used for predicting	Small Phytoplankton	PI Control	-	-	-	-	-	-
			4x CO <sub>2</sub>	(0.829) 0.9887	(0.829) 0.9874	(0.9287) 0.9902	-	-	-
			3x Mixing	(0.9287) 0.9901	(0.788) 0.9849	-	-	-	-
		Large Phytoplankton	PI Control	-	-	-	-	(0.7842) 0.9683	(0.8831) 0.9772
			4x CO <sub>2</sub>	-	-	-	(0.7842) 0.9722	-	(0.7306) 0.969
			3x Mixing	-	-	-	(0.8831) 0.9738	(0.7306) 0.963	-
<b>RMSE</b>	NNE being used for predicting	Small Phytoplankton	PI Control	-	( $3.06 \times 10^{-9}$ ) $7.38 \times 10^{-10}$	( $1.84 \times 10^{-9}$ ) $6.55 \times 10^{-10}$	-	-	-
			4x CO <sub>2</sub>	( $3.06 \times 10^{-9}$ ) $7.15 \times 10^{-10}$	-	( $3.56 \times 10^{-9}$ ) $7.3 \times 10^{-10}$	-	-	-
			3x Mixing	( $1.84 \times 10^{-9}$ ) $6.64 \times 10^{-10}$	( $3.56 \times 10^{-9}$ ) $7.97 \times 10^{-10}$	-	-	-	-
		Large Phytoplankton	PI Control	-	-	-	-	( $1 \times 10^{-9}$ ) $3.11 \times 10^{-9}$	( $7.34 \times 10^{-9}$ ) $3.2 \times 10^{-9}$
			4x CO <sub>2</sub>	-	-	-	( $1 \times 10^{-9}$ ) $3.44 \times 10^{-9}$	-	( $1.17 \times 10^{-9}$ ) $3.74 \times 10^{-9}$
			3x Mixing	-	-	-	( $7.34 \times 10^{-9}$ ) $3.34 \times 10^{-9}$	( $1.17 \times 10^{-9}$ ) $3.33 \times 10^{-9}$	-
<b>Percent Decrease in Error</b>	NNE being used for predicting	Small Phytoplankton	PI Control	-	75.90%	64.45%	-	-	
			4x CO <sub>2</sub>	76.66%	-	79.53%	-	-	
			3x Mixing	63.98%	77.64%	-	-	-	
		Large Phytoplankton	PI Control	-	-	-	-	69.09%	56.32%
			4x CO <sub>2</sub>	-	-	-	65.71%	-	67.99%
			3x Mixing	-	-	-	54.45%	71.50%	-

(Table 3). This implies the NNEs applied to the other runs [were](#) better able to predict the outcome than the point-by-point analysis, once again reinforcing our previous result.

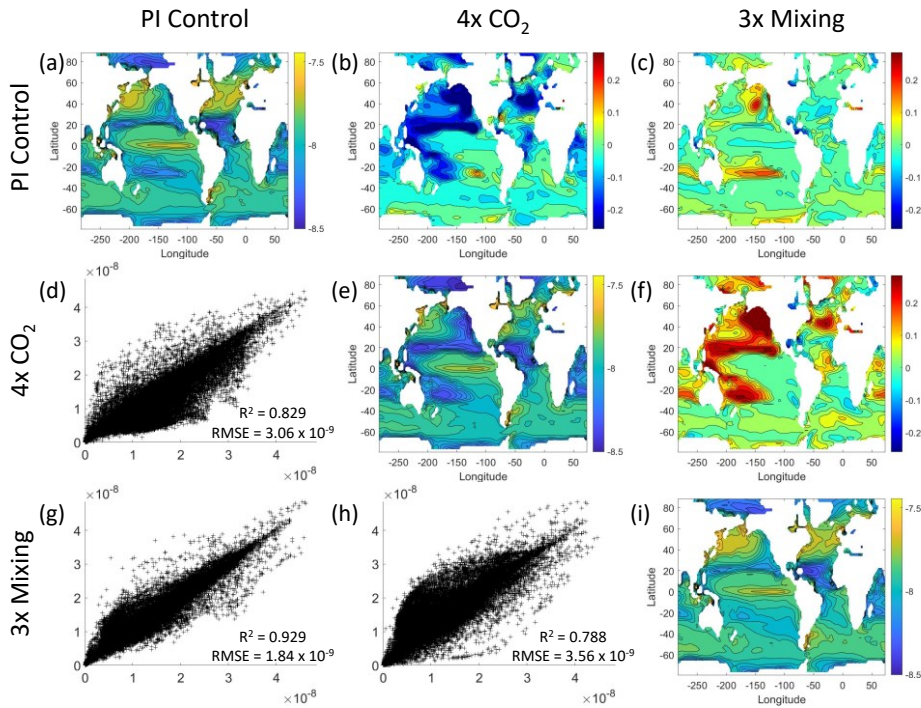


**Figure 5:** Comparison of the model runs for small phytoplankton biomass in Case 1. The units for biomass in all subplots are  $\text{mol kg}^{-1}$ . The subplots show point-by-point scatter plots comparing the model runs against one another (d, g, h), yearly averaged log10 biomass plots for each model run (a, e, i), and the log10 relative ratios comparing the yearly averaged contour plots of the model runs (b, c, f). The x-axis and y-axis of the scatter plots (d, g, h) correspond to the horizontal/vertical model run labels, respectively (ex. Box (d) shows PI Control on the x-axis and 4xCO<sub>2</sub> on the y-axis). The yearly averaged log10 contour plots (a, e, i) correspond to the matching horizontal/vertical model run labels (ex. Box (a) shows the yearly averaged log10 biomass of PI Control). The log10 relative ratios (b, c, f) were calculated as the model run listed on the horizontal axis divided by the model run listed on the vertical axis (ex. Box (b) shows 4xCO<sub>2</sub> divided PI Control).

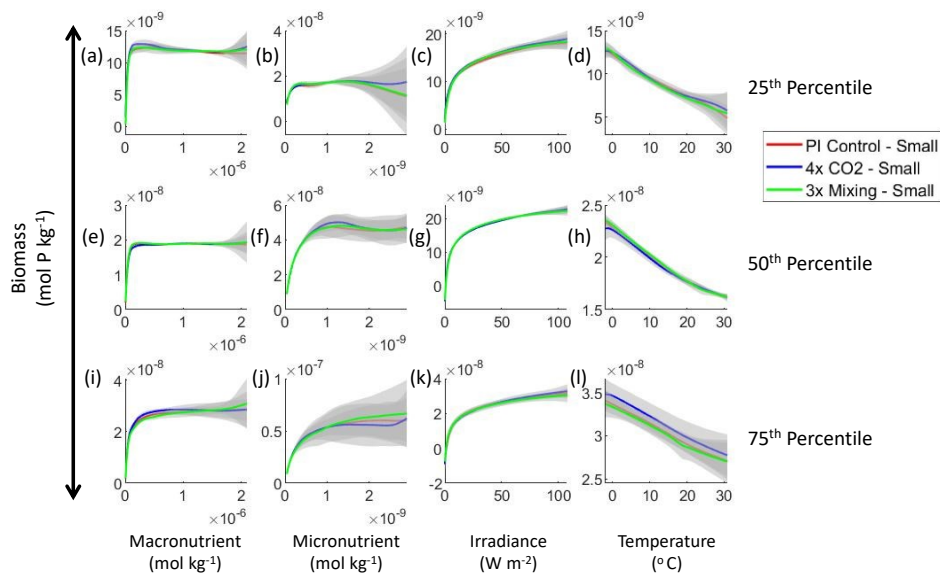


**Figure 4:** Sensitivity analysis plots for the small phytoplankton of Case 1. This figure is provided to allow for examination of the apparent relationships for the small phytoplankton, since the large phytoplankton apparent relationships made it difficult to see those for the small phytoplankton in Fig. 3. Each line is the prediction for the NNE (i.e., the average prediction of 25 NNs) specific to each model run and the color of each line represents the model run (PI Control – Red; 4xCO<sub>2</sub> – Blue; 3xMixing - Green). The gray region around each line shows one standard deviation in the predictions of the individual NNs that make up each NNE (e.g., the gray region around the solid red curves shows the standard deviation in the predictions of the 25 NNs that make up that particular NNE). The rows correspond to the percentile value at which the other predictor variables were held constant (e.g., box (a) varies the macronutrient across its min-max range and holds the micronutrient, irradiance, and temperature at their respective 25th percentile values). Columns show the x-axis variables as they vary between their min-max range. The y-axis in all subplots is the biomass concentration. Note that the biomass scale changes with each subplot.

That the NNEs from one model run **were** able to reproduce the results from the other model runs **was** not simply due to the models producing similar spatiotemporal patterns. To ensure that distinct differences between the model runs **were** present, we **compared** each model run against the others (Fig. 5 and 6). Differences in the biomass values between the three model runs **were** evident (Fig. 5 and 6). First, we **compared** each model run against the others in a point-by-point analysis and **observed** that different biomasses **were** occurring at the same spatiotemporal locations (Fig. 5 and 6 d, g, h). For example, in the small phytoplankton scatter plot for PI

415

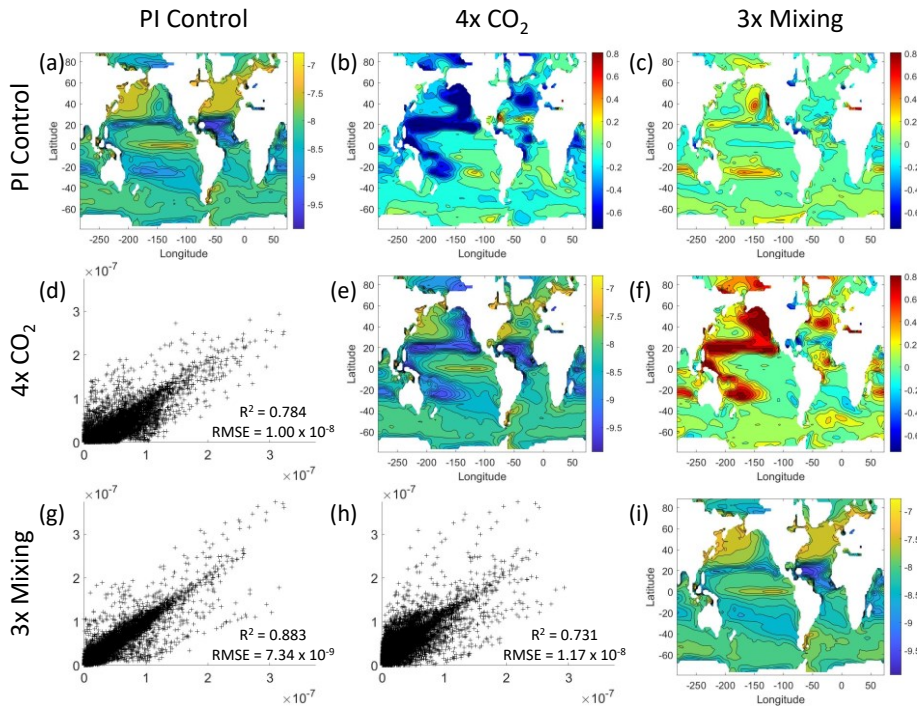


**Figure 6:** Comparison of the model runs for large phytoplankton biomass in Case 1. The units for biomass in all subplots are  $\text{mol kg}^{-1}$ . The subplots show point-by-point scatter plots comparing the model runs against one another (d, g, h), yearly averaged log10 biomass plots for each model run (a, e, i), and the log10 relative ratios comparing the yearly averaged contour plots of the model runs (b, c, f). The x-axis and y-axis of the scatter plots (d, g, h) correspond to the horizontal/vertical model run labels, respectively (ex. Box (d) shows PI Control on the x-axis and 4xCO<sub>2</sub> on the y-axis). The yearly averaged log10 contour plots (a, e, i) correspond to the matching horizontal/vertical model run labels (ex. Box (a) shows the yearly averaged log10 biomass of PI Control). The log10 relative ratios (b, c, f) were calculated as the model run listed on the horizontal axis divided by the model run listed on the vertical axis (ex. Box (b) shows 4xCO<sub>2</sub> divided PI Control).

Control vs 4xCO<sub>2</sub>, PI Control ~~showed~~shows a tendency of having higher biomass values than 4xCO<sub>2</sub> across most locations (Fig. 5 d). Additionally, we ~~looked~~look at the contour plots and ~~log~~log10 relative ratios using the yearly averaged biomass for each case (Fig. 5 and 6 a-c, e, f, i). Specific large differences that we ~~noted~~were~~note~~ are higher biomass in the Pacific and Northern Atlantic in PI Control and 3xMixing relative to 4xCO<sub>2</sub> (Fig. 5 and 6 b, f) and the highest biomass ~~in~~occurring in 3xMixing in the subtropical regions of the Pacific (Fig. 5 and 6 c). Similar patterns ~~were~~are observed in the large phytoplankton, as well (Fig. 6). These differences between the model runs are relatively

Formatted: Subscript

Formatted: Subscript

420



**Table 3:** The performance metrics for the NNEs being used to predict the outcome of the other model runs for the same size class of Case 1. In the top half of the table, the R-squared and RMSE are listed. The values in parentheses are the values from comparing the respective cases against one another (these are the same values listed in the respective scatter plots of Fig. 5 and 6). The values outside the parentheses are the values from using the trained NNE of the model listed in the row to predict the outcome of the model run in the column (e.g., the NNE trained on 4xCO<sub>2</sub> was used to predict the PI Control outcome using the predictor values of PI Control. These values were compared against the actual values of the PI Control to compute the RMSE of  $7.15 \times 10^{-10}$ ). In the bottom half of the table is the percent decrease in RMSE from the number listed inside the parentheses to the RMSE outside the parentheses.

		Case being predicted									
		Small Phytoplankton			Large Phytoplankton						
		PI Control	4x CO <sub>2</sub>	3x Mixing	PI Control	4x CO <sub>2</sub>	3x Mixing				
<b>R-squared</b>	NNE being used for predicting	Small Phytoplankton	PI Control	-	(0.829) 0.9874	(0.9287) 0.9902	-	-	-	-	-
			4x CO <sub>2</sub>	(0.829) 0.9887	-	(0.788) 0.9878	-	-	-	-	-
			3x Mixing	(0.9287) 0.9901	(0.788) 0.9849	-	-	-	-	-	-
		Large Phytoplankton	PI Control	-	-	-	(0.7842) 0.9722	(0.7842) 0.9683	(0.8831) 0.9772	-	-
			4x CO <sub>2</sub>	-	-	-	(0.8831) 0.9738	(0.7306) 0.963	(0.7306) 0.969	-	-
			3x Mixing	-	-	-	-	-	-	-	-
<b>RMSE</b>	NNE being used for predicting	Small Phytoplankton	PI Control	-	( $3.06 \times 10^{-9}$ ) $7.38 \times 10^{-10}$	( $1.84 \times 10^{-9}$ ) $6.55 \times 10^{-10}$	-	-	-	-	
			4x CO <sub>2</sub>	( $3.06 \times 10^{-9}$ ) $7.15 \times 10^{-10}$	-	( $3.56 \times 10^{-9}$ ) $7.3 \times 10^{-10}$	-	-	-	-	
			3x Mixing	( $1.84 \times 10^{-9}$ ) $6.64 \times 10^{-10}$	( $3.56 \times 10^{-9}$ ) $7.97 \times 10^{-10}$	-	-	-	-	-	
		Large Phytoplankton	PI Control	-	-	-	( $1 \times 10^{-9}$ ) $3.11 \times 10^{-9}$	( $7.34 \times 10^{-9}$ ) $3.2 \times 10^{-9}$	-	-	
			4x CO <sub>2</sub>	-	-	-	( $1 \times 10^{-9}$ ) $3.44 \times 10^{-9}$	-	( $1.17 \times 10^{-9}$ ) $3.74 \times 10^{-9}$	-	
			3x Mixing	-	-	-	( $7.34 \times 10^{-9}$ ) $3.34 \times 10^{-9}$	( $1.17 \times 10^{-9}$ ) $3.33 \times 10^{-9}$	-	-	
<b>Percent Decrease in Error</b>	NNE being used for predicting	Small Phytoplankton	PI Control	-	75.90%	64.45%	-	-	-	-	
			4x CO <sub>2</sub>	76.66%	-	79.53%	-	-	-	-	
			3x Mixing	63.98%	77.64%	-	-	-	-	-	
		Large Phytoplankton	PI Control	-	-	-	69.09%	56.32%	-	-	
			4x CO <sub>2</sub>	-	-	-	65.71%	-	67.99%	-	
			3x Mixing	-	-	-	54.45%	71.50%	-	-	

large (exceeding a factor of three in some locations) and allow us to dismiss the possibility that the similar apparent relationships were only due to strong similarities between the model runs.

Although the sensitivity analysis allowed us to see that the apparent relationships were the same for each size class, it also allows us to see how the two size classes react differently to the same conditions. Most notably, the large phytoplankton seem to be very sensitive to the micronutrient compared to the small phytoplankton (Fig. 3; closer view of small phytoplankton in Fig. 4). When the other predictors are held at their 75<sup>th</sup> percentile values (high macronutrient, high irradiance, and warm temperature), the large phytoplankton are able to reach biomass values almost an order of magnitude higher than the small phytoplankton (Fig. 3 and 4 j). This is what would be expected given the cubic relationship of large phytoplankton with growth rate. Another interesting relationship is the stark asymptotes in both size classes of the macronutrient plots, suggesting limitations by other nutrients, likely the micronutrient (Fig. 3 a, e, i). One unexpected relationship was the decreasing biomass with increasing temperature in both size classes (Fig. 3 d, h, l). This could be a result of warmer regions having less available nutrients or because of the temperature

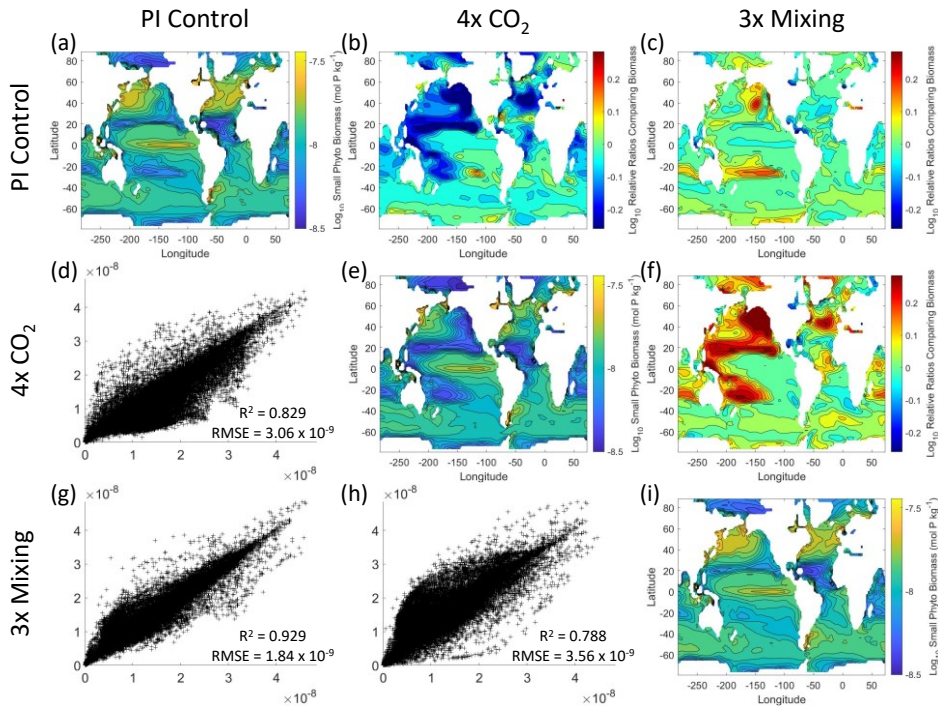


**Figure 5:** Comparison of the model runs for small phytoplankton biomass in Case 1. The units for biomass in all subplots are mol P kg<sup>-1</sup>. The subplots show point-by-point scatter plots comparing the model runs against one another (d, g, h), yearly averaged log<sub>10</sub> biomass plots for each model run (a, e, i), and the log<sub>10</sub> relative ratios comparing the yearly averaged contour plots of the model runs (b, c, f). The x-axis and y-axis of the scatter plots (d, g, h) correspond to the horizontal/vertical model run labels, respectively (e.g., box (d) shows PI Control on the x-axis and 4xCO<sub>2</sub> on the y-axis). The yearly averaged log<sub>10</sub> contour plots (a, e, i) correspond to the matching horizontal/vertical model run labels (e.g., box (a) shows the yearly averaged log<sub>10</sub> biomass of PI Control). The log<sub>10</sub> relative ratios (b, c, f) were calculated as the model run listed on the horizontal axis divided by the model run listed on the vertical axis (e.g., box (b) shows 4xCO<sub>2</sub> divided PI Control).

dependent chlorophyll-to-carbon (Chl:C) ratios (Geider et al., 1997) which would lead to phytoplankton needing more light higher irradiance in warmer waters.

440 Relative to our main objective in Case 1 to quantify the extent to which differences in physical circulation affect the apparent relationships, our results indicated indicate that the different physical circulations diddo not produce differences in the apparent relationships found by NNEs. When the biological equations remainedremain the same,

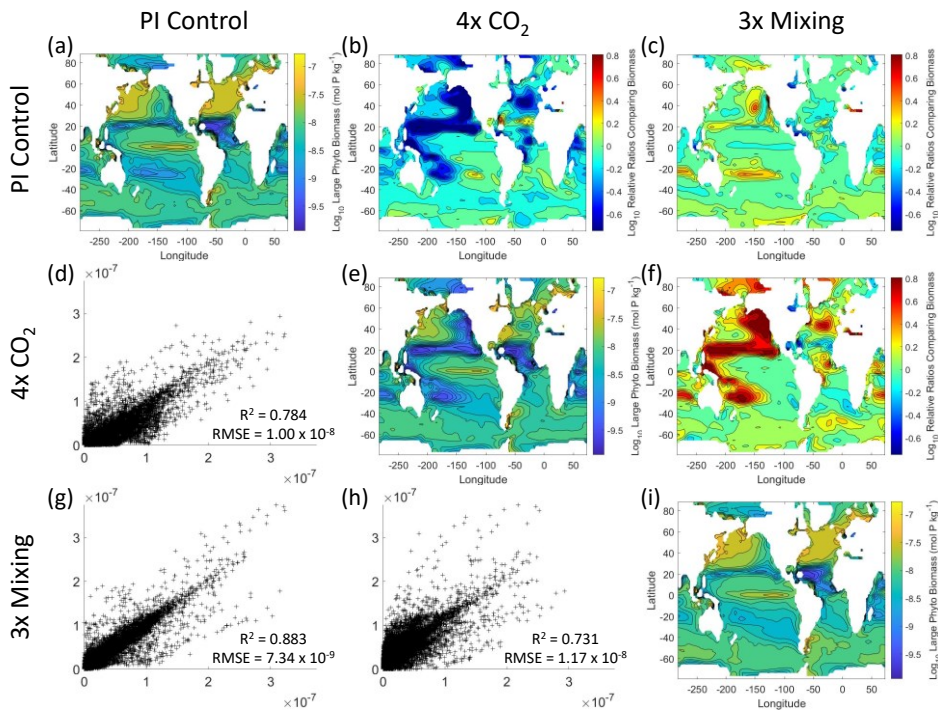


**Figure 6:** Comparison of the model runs for large phytoplankton biomass in Case 1. The units for biomass in all subplots are mol P kg<sup>-1</sup>. The subplots show point-by-point scatter plots comparing the model runs against one another (d, g, h), yearly averaged log<sub>10</sub> biomass plots for each model run (a, e, i), and the log<sub>10</sub> relative ratios comparing the yearly averaged contour plots of the model runs (b, c, f). The x-axis and y-axis of the scatter plots (d, g, h) correspond to the horizontal/vertical model run labels, respectively (e.g., box (d) shows PI Control on the x-axis and 4xCO<sub>2</sub> on the y-axis). The yearly averaged log<sub>10</sub> contour plots (a, e, i) correspond to the matching horizontal/vertical model run labels (e.g., box (a) shows the yearly averaged log<sub>10</sub> biomass of PI Control). The log<sub>10</sub> relative ratios (b, c, f) were calculated as the model run listed on the horizontal axis divided by the model run listed on the vertical axis (e.g., box (b) shows 4xCO<sub>2</sub> divided PI Control).

changing the physical parameters simply **changed** where combinations of nutrients and **light occurred**. The NNEs can find the same apparent relationships between the model runs when the equations and constants governing those runs are identical, even if the inputs differ. In contrast to changes in nutrients, changes in biomass in the BLING ESM **were** not a function of the physical circulation.

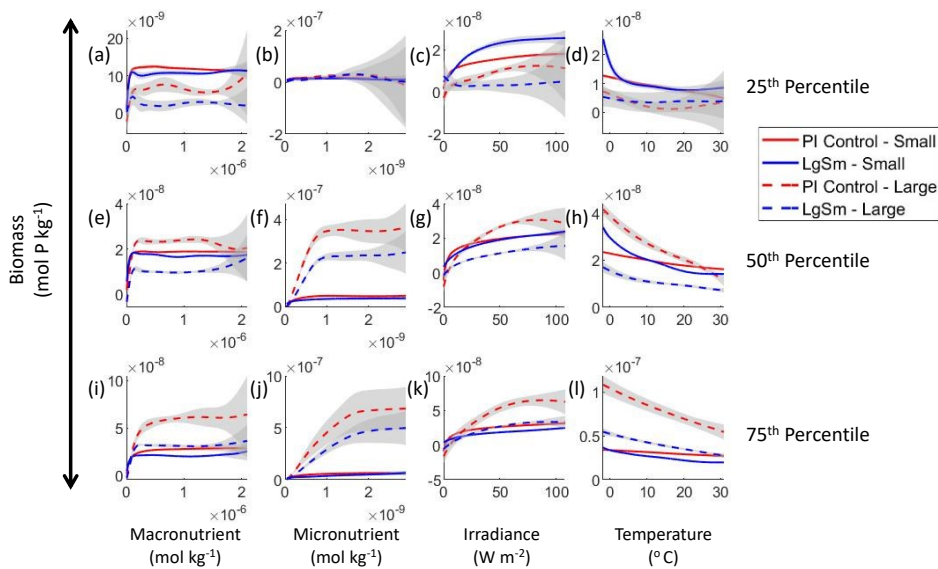


**Figure 7:** Sensitivity analysis plots for the small and large phytoplankton of Case 2. Each line is the prediction for the NNE (i.e., the average prediction of 25 NNs) specific to each model run and the color of each line represents the model run (PI Control – Red; LgSm – Blue). The solid lines correspond to the small phytoplankton and the dashed lines to the large phytoplankton. The gray region around each line shows one standard deviation in the predictions of the individual NNs that make up each NNE (e.g., the gray region around the solid red curves shows the standard deviation in the predictions of the 25 NNs that make up that particular NNE). The rows correspond to the percentile value at which the other predictor variables were held constant (e.g., box (a) varies the macronutrient across its min-max range and holds the micronutrient, irradiance, and temperature at their respective 25<sup>th</sup> percentile values). Columns show the x-axis variables as they vary between their min-max range. The y-axis in all subplots is the biomass concentration. Note that the biomass scale changes with each subplot.

#### 4.2 Case 2 – Same ESM: Different Diagnostic Biological Equations, Near-Identical Physical Circulations

In Case 1, it **was** clear from our results that when the biological cycling **was** identical between model runs, the NNEs **found** the same apparent relationships because the biomass **was** not a function of the physical circulation. Since the biomass is clearly a function of the biological equations, it would be reasonable to assume that the apparent relationships **would** be different between model runs that are governed by different biological equations. So, for Case 2, the objective **was** to quantify the extent to which NNEs **could** detect differences in the apparent relationships when the intrinsic biological relationships between model runs **were** different, while maintaining

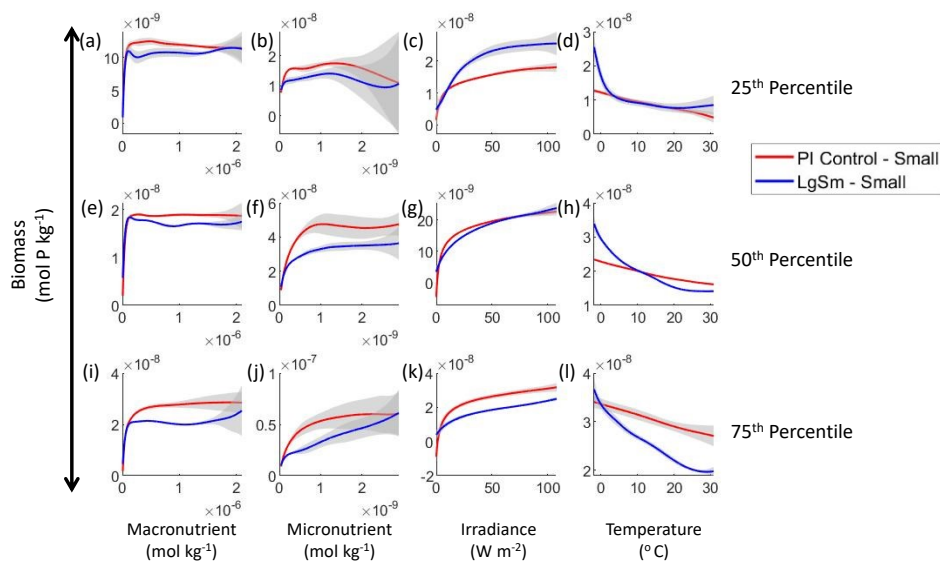


**Figure 8:** Sensitivity analysis plots for the small phytoplankton of Case 2. This figure is provided to allow for examination of the apparent relationships for the small phytoplankton, since the large phytoplankton apparent relationships made it difficult to see those for the small phytoplankton in Fig. 7. Each line is the prediction for the NNE (i.e., the average prediction of 25 NNs) specific to each model run and the color of each line represents the model run (PI Control – Red; LgSm – Blue). The gray region around each line shows one standard deviation in the predictions of the individual NNs that make up each NNE (e.g., the gray region around the solid red curves shows the standard deviation in the predictions of the 25 NNs that make up that particular NNE). The rows correspond to the percentile value at which the other predictor variables were held constant (e.g., box (a) varies the macronutrient across its min-max range and holds the micronutrient, irradiance, and temperature at their respective 25<sup>th</sup> percentile values). Columns show the x-axis variables as they vary between their min-max range. The y-axis in all subplots is the biomass concentration. Note that the biomass scale changes with each subplot.

455 similar physical circulations and still using a diagnostic model which guarantees that identical nutrient, ~~high~~ irradiance, and temperature at two different points will produce identical biomass.

Our results show that NNEs can differentiate the apparent relationships between model runs when the biological equations differ. The sensitivity analysis for Case 2 shows that different apparent relationships ~~were~~ ~~are~~ found between model runs and within the same size classes, relative to the non-overlapping gray standard deviation regions around each line (Fig. 7 and 8). Additionally, we can be fairly confident in these predictions given the high-performance

460

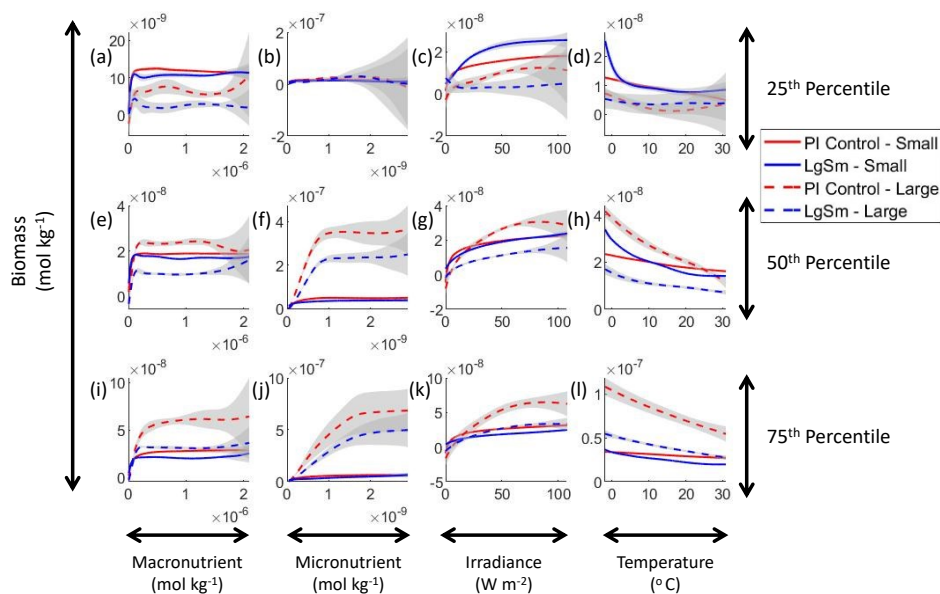


**Figure 7:** Sensitivity analysis plots for the small and large phytoplankton of Case 2. Each line is the prediction for the NNE specific to each model run and the color of each line represents the model run (PI Control—Red; LgSm—Blue). The solid lines correspond to the small phytoplankton and the dashed lines to the large phytoplankton. The gray region around each line shows one standard deviation in the predictions of the individual NNs that make up each NNE (ex. The gray region around the solid red curves shows the standard deviation in the predictions of the 25 NNs that make up that particular NNE). The rows correspond to the percentile value at which the other predictor variables were held constant (ex. Box (a) varies the macronutrient across its min-max range and holds the micronutrient, irradiance, and temperature at their respective 25<sup>th</sup> percentile values). Columns show the x-axis variables as they vary between their min-max range. The y-axis in all subplots is the biomass concentration. Note that the biomass scale changes with each subplot.

metrics in both the training and testing subsets (highest RMSE =  $3.11 \times 10^{-9}$  mol P kg<sup>-1</sup> [Table 2] vs. the average total biomass of  $1.36 \times 10^{-8}$  mol P kg<sup>-1</sup>).

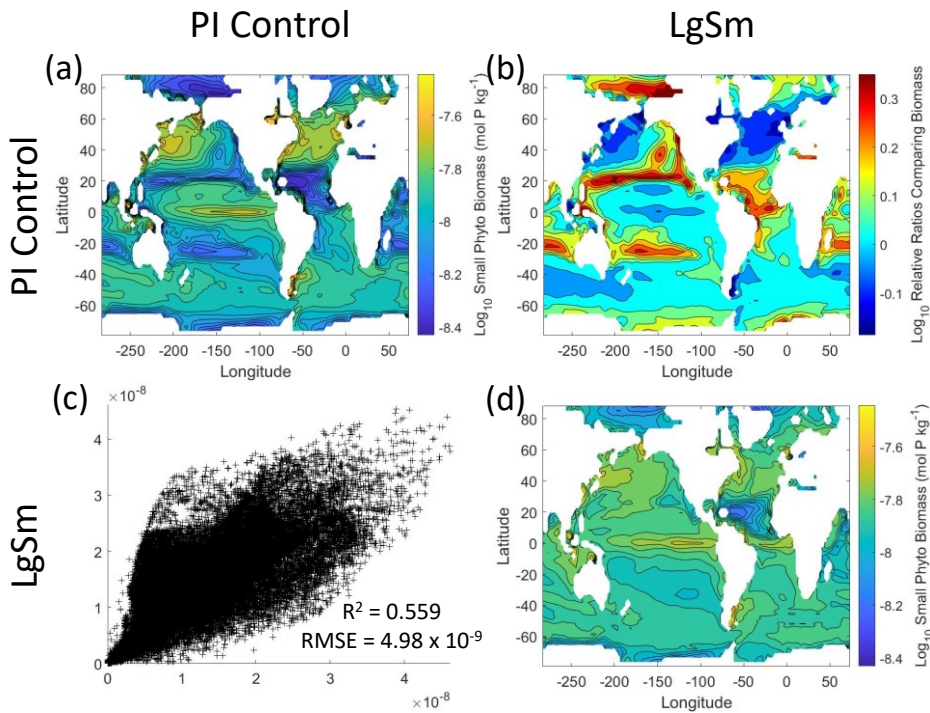


**Figure 9:** Comparison of the model runs for small phytoplankton biomass in Case 2. The units for biomass in all subplots are mol P kg<sup>-1</sup>. The subplots show point-by-point scatter plots comparing the model runs against one another (c), yearly averaged log10 biomass plots for each model run (a and d), and the log10 relative ratios comparing the yearly averaged contour plots of the model runs (b). The x-axis and y-axis of the scatter plots (c) correspond to the horizontal/vertical model run labels, respectively (e.g., box (c) shows PI Control on the x-axis and LgSm on the y-axis). The yearly averaged log10 contour plots (a and d) correspond to the matching horizontal/vertical model run labels (e.g., box (a) shows the yearly averaged log10 biomass of PI Control). The log10 relative ratios (b) were calculated as the model run listed on the horizontal axis divided by the model run listed on the vertical axis (e.g., box (b) shows LgSm divided PI Control).

This result of different relationships, when the model runs are governed by different biological equations, reinforces what we found in Case 1. Changing the biological equations can be likened to changing how the nutrients affect the phytoplankton biomass (the function  $g(N_{J,LL,LL2})$  in Fig. 1). While it might seem obvious that changing the biological equations will change the biomass values, it **remained** unclear whether NNEs would be able to pick out these differences in the apparent relationships.

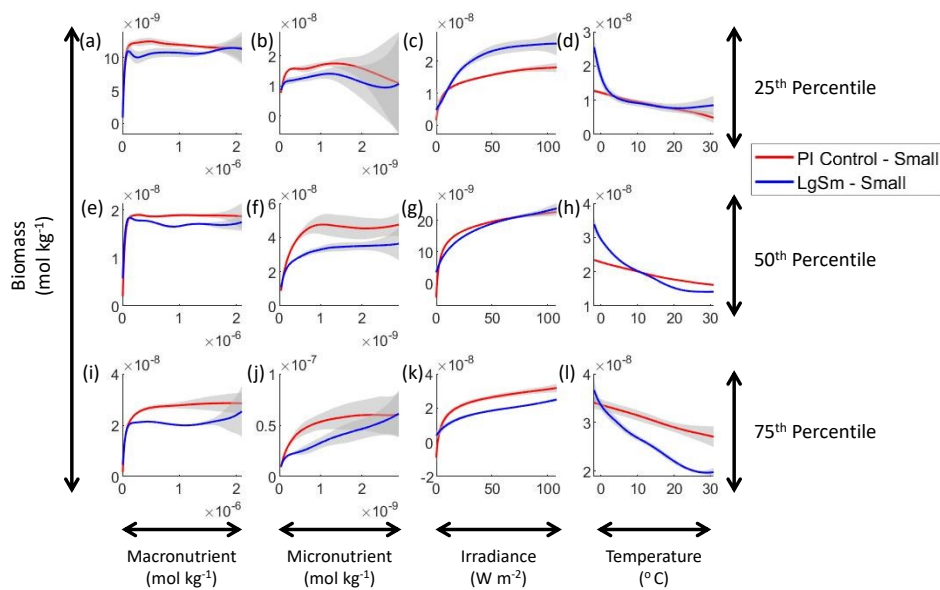


**Figure 8:** Sensitivity analysis plots for the small phytoplankton of Case 2. This figure is provided to allow for examination of the apparent relationships for the small phytoplankton, since the large phytoplankton apparent relationships made it difficult to see those for the small phytoplankton in Fig. 7. Each line is the prediction for the NNE specific to each model run and the color of each line represents the model run (PI Control—Red; LgSm—Blue). The gray region around each line shows one standard deviation in the predictions of the individual NNs that make up each NNE (ex. The gray region around the solid red curves shows the standard deviation in the predictions of the 25 NNs that make up that particular NNE). The rows correspond to the percentile value at which the other predictor variables were held constant (ex. Box (a) varies the macronutrient across its min-max range and holds the micronutrient, irradiance, and temperature at their respective 25<sup>th</sup> percentile values). Columns show the x axis variables as they vary between their min-max range. The y axis in all subplots is the biomass concentration. Note that the biomass scale changes with each subplot.



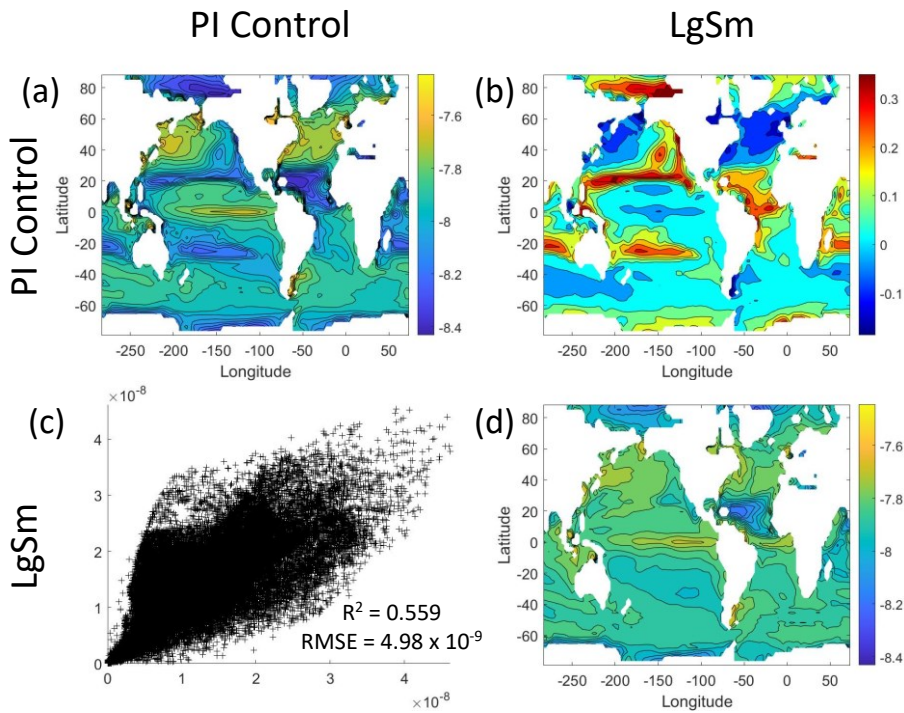


**Figure 9:** Comparison of the model runs for small phytoplankton biomass in Case 2. The units for biomass in all subplots are  $\text{mol kg}^{-1}$ . The subplots show point-by-point scatter plots comparing the model runs against one another (c), yearly-averaged  $\log_{10}$  biomass plots for each model run (a and d), and the  $\log_{10}$  relative ratios comparing the yearly-averaged contour plots of the model runs (b). The x axis and y axis of the scatter plots (c) correspond to the horizontal/vertical model run labels, respectively (ex. Box (c) shows PI Control on the x axis and LgSm on the y axis). The yearly-averaged  $\log_{10}$  contour plots (a and d) correspond to the matching horizontal/vertical model run labels (ex. Box (a) shows the yearly-averaged  $\log_{10}$  biomass of PI Control). The  $\log_{10}$  relative ratios (b) were calculated as the model run listed on the horizontal axis divided by the model run listed on the vertical axis (ex. Box (b) shows LgSm divided PI Control).

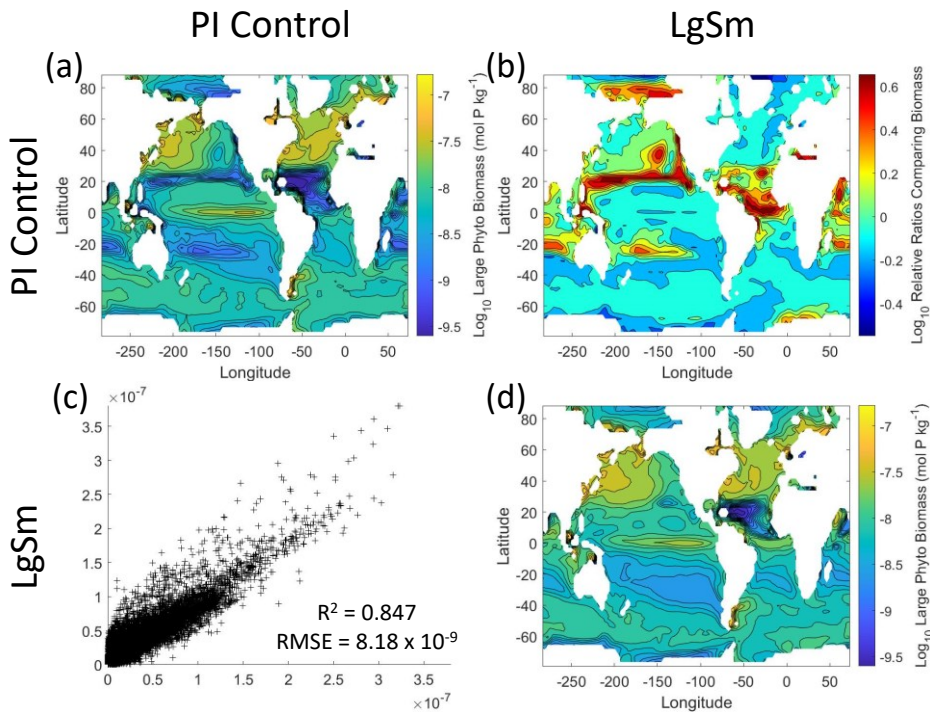


**Figure 10:** Comparison of the model runs for large phytoplankton biomass in Case 2. The units for biomass in all subplots are mol P kg<sup>-1</sup>. The subplots show point-by-point scatter plots comparing the model runs against one another (c), yearly averaged log<sub>10</sub> biomass plots for each model run (a and d), and the log<sub>10</sub> relative ratios comparing the yearly averaged contour plots of the model runs (b). The x-axis and y-axis of the scatter plots (c) correspond to the horizontal/vertical model run labels, respectively (e.g., box (c) shows PI Control on the x-axis and LgSm on the y-axis). The yearly averaged log<sub>10</sub> contour plots (a and d) correspond to the matching horizontal/vertical model run labels (e.g., box (a) shows the yearly averaged log<sub>10</sub> biomass of PI Control). The log<sub>10</sub> relative ratios (b) were calculated as the model run listed on the horizontal axis divided by the model run listed on the vertical axis (e.g., box (b) shows LgSm divided PI Control).

We ~~wanted~~want to ensure there ~~were~~are noticeable differences between the model runs (Fig. 9 and 10). We did this in Case 1 to ensure that the similar apparent relationships found by the NNEs were not simply because of similarities in the model output. In Case 2, the difference in model outputs serves to reinforce the different apparent relationships found by the NNEs. In the point-by-point comparison, the large phytoplankton ~~showed~~show more agreement between model runs (Fig. 10 c) than the small phytoplankton (Fig. 9 c). However, when we ~~examined~~examine the contour and

Formatted: English (United States)

Formatted: English (United States)

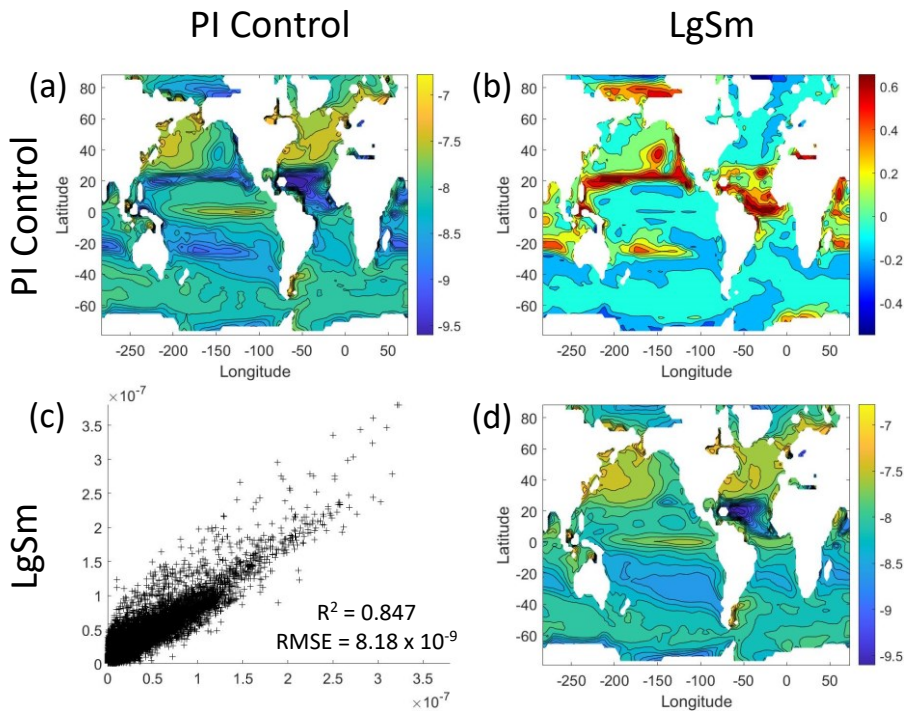


**Figure 10:** Comparison of the model runs for large phytoplankton biomass in Case 2. The units for biomass in all subplots are mol kg<sup>-1</sup>. The subplots show point-by-point scatter plots comparing the model runs against one another (c), yearly-averaged log<sub>10</sub> biomass plots for each model run (a and d), and the log<sub>10</sub> relative ratios comparing the yearly-averaged contour plots of the model runs (b). The x axis and y axis of the scatter plots (c) correspond to the horizontal/vertical model run labels, respectively (ex. Box (c) shows PI Control on the x axis and LgSm on the y axis). The yearly-averaged log<sub>10</sub> contour plots (a and d) correspond to the matching horizontal/vertical model run labels (ex. Box (a) shows the yearly-averaged log<sub>10</sub> biomass of PI Control). The log<sub>10</sub> relative ratios (b) were calculated as the model run listed on the horizontal axis divided by the model run listed on the vertical axis (ex. Box (b) shows LgSm divided PI Control).

log<sub>10</sub> relative ratios (Fig. 9 and 10 a, b, d), it was evident that clear, large, systematic, spatially coherent differences existed between the model runs. Both the small and large phytoplankton showed higher concentrations in the LgSm model run compared to PI Control for the subtropical and polar regions of the Pacific and Indian Oceans, along with higher concentrations in the equatorial Atlantic (Fig. 9 and 10-b).

480

**Table 4:** The performance metrics for the NNEs being used to predict the outcome of the other model runs for the same size class of Case 2. In the top half of the table, the R-squared and RMSE are listed. The values in parentheses are the values from comparing the respective cases against one another (these are the same values listed in the respective scatter plots of Fig. 9 and 10). The values outside the parentheses are the values from using the trained NNE of the model listed in the row to predict the outcome of the model run in the column (e.g., the NNE trained on LgSm was used to predict the PI Control outcome using the predictor values of PI Control. These values were compared against the actual values of the PI Control to compute the RMSE of  $3.07 \times 10^{-9}$ ). In the bottom half of the table is the percent decrease in RMSE from the number listed inside the parentheses to the RMSE outside the parentheses (a negative percent means that the error increased).

				Case being predicted			
				Small Phytoplankton		Large Phytoplankton	
				PI Control	LgSm	PI Control	LgSm
R-squared	NNE being used for predicting	Small Phytoplankton	PI Control	-	(0.5591) 0.8192	-	-
			LgSm	(0.5591) 0.7899	-	-	-
		Large Phytoplankton	PI Control	-	-	(0.8465) 0.9334	-
			LgSm	-	-	(0.8465) 0.9171	-
RMSE	NNE being used for predicting	Small Phytoplankton	PI Control	-	( $4.98 \times 10^{-9}$ ) $3.95 \times 10^{-9}$	-	-
			LgSm	( $4.98 \times 10^{-9}$ ) $3.07 \times 10^{-9}$	-	-	-
		Large Phytoplankton	PI Control	-	-	( $8.18 \times 10^{-9}$ ) $1.56 \times 10^{-8}$	-
			LgSm	-	-	( $8.18 \times 10^{-9}$ ) $1.01 \times 10^{-8}$	-
Percent Decrease in Error	NNE being used for predicting	Small Phytoplankton	PI Control	-	20.59%	-	-
			LgSm	38.20%	-	-	-
		Large Phytoplankton	PI Control	-	-	-	-90.87%
			LgSm	-	-	-23.11%	-

Although the gray regions in Figs. 7 and 8 overlap toward the higher concentrations of each predictor, this is likely due to the lack of observations in the training data meeting ~~that~~ those criteria, without which the NNEs ~~could not~~ cannot be constrained. For example, in Fig. 7 (j), the apparent relationships of the large phytoplankton overlap past about ~~5~~  $5 \times 10^{-10}$  mol kg<sup>-1</sup> of the micronutrient, because there ~~were~~ are no observations in the training data that ~~were~~ are greater than ~~5~~  $5 \times 10^{-10}$  mol kg<sup>-1</sup> of the micronutrient while simultaneously being at the 75<sup>th</sup> percentile level of the macronutrient, irradiance, and temperature (data not shown). Without observations to constrain them, the NNEs ~~were~~ ~~unable to~~ cannot be constrained and, therefore, ~~are~~ less certain about the ~~extrapolated~~ relationships in those regions which ~~lead~~ leads to higher uncertainty and overlapping standard deviations.

As in Case 1, our result ~~was~~ is supported by the additional test in which the NNEs trained on one model run ~~were~~ are tasked with making predictions on the other. Had the NNEs found similar apparent relationships, the reductions in error would have been of similar magnitude as those in Case 1 (Table 3 vs Table 4). For this second case, we ~~saw~~ see that there ~~were~~ are only modest decreases in RMSE for the small phytoplankton and increases in RMSE for large phytoplankton (Table 4). For example, relative to the RMSE of the point-by-point comparison, the RMSE ~~decreased~~ decreases about 21% when LgSm ~~made~~ makes predictions on PI Control for the small phytoplankton (Table

4). Additionally, it ~~was~~is observed that even though the RMSE ~~increased~~increases in the large phytoplankton, the R<sup>2</sup> values ~~improved~~improve in the cross-model comparison compared to the point-by-point comparison (0.92-0.93 vs 0.85; Table 4). This suggests that the NNEs ~~improved~~improve the simulation in terms of the overall pattern, but not the magnitude. These results make sense since the apparent relationships of the small phytoplankton ~~showed~~show greater similarities than the apparent relationships of the large phytoplankton (Fig. 7).

With respect to the apparent relationships that the NNEs ~~uncovered~~uncover, the large phytoplankton once again ~~appeared~~appear to be more sensitive to the micronutrient concentrations compared to the small phytoplankton (Fig. 7 b, f, j). Both size classes ~~showed~~show asymptotes around the same concentrations for the macronutrient, albeit at different biomass values (Fig. 7 a, c, i). As with Case 1, the decreasing biomass with increasing temperature ~~was~~is an unexpected relationship (Fig. 7 d, h, l), which might be explained by the temperature dependent Chl:C ratios causing phytoplankton in warmer regions to need ~~more light~~higher irradiance.

~~Our~~As previously stated, our main objective with Case 2 ~~was~~is to quantify the extent to which NNEs ~~could~~can detect differences in the apparent relationships when the physical conditions between model runs ~~were~~are identical and the biological relationships ~~differed~~differ. With the biomass being a function of changes in biomass from biology (~~ie~~i.e. the equations governing how nutrients affect biomass), ~~it is unsurprising that~~it is unsurprising that different biological equations ~~produced~~produce differences in biomass. What was unclear was whether NNEs would be able to highlight these differences in the apparent relationships. Our results indicate that NNEs ~~could~~can find noticeable differences in the apparent relationships, insofar as the standard deviation ~~regions did not often overlap in~~region of the sensitivity analysis curves ~~do not overlap~~do not overlap.

**Table 4:** The performance metrics for the NNEs being used to predict the outcome of the other model runs for the same size class of Case 2. In the top half of the table, the R-squared and RMSE are listed. The values in parentheses are the values from comparing the respective cases against one another (these are the same values listed in the respective scatter plots of Fig. 9 and 10). The values outside the parentheses are the values from using the trained NNE of the model listed in the row to predict the outcome of the model run in the column (ex. The NNE trained on LgSm was used to predict the PI Control outcome using the predictor values of PI Control. These values were compared against the actual values of the PI Control to compute the RMSE of  $3.07 \times 10^{-9}$ ). In the bottom half of the table is the percent decrease in RMSE from the number listed inside the parentheses to the RMSE outside the parentheses (a negative percent means that the error increased).

		Case being predicted					
		Small Phytoplankton		Large Phytoplankton			
		PI Control	LgSm	PI Control	LgSm		
<b>R-squared</b>	NNE being used for predicting	Small Phytoplankton	PI Control	-	(0.5591) 0.8192	-	-
			LgSm	(0.5591) 0.7899	-	-	-
		Large Phytoplankton	PI Control	-	-	-	(0.8465) 0.9334
			LgSm	-	-	(0.8465) 0.9171	-
<b>RMSE</b>	NNE being used for predicting	Small Phytoplankton	PI Control	-	( $4.98 \times 10^{-9}$ ) $3.95 \times 10^{-9}$	-	-
			LgSm	( $4.98 \times 10^{-9}$ ) $3.07 \times 10^{-9}$	-	-	-
		Large Phytoplankton	PI Control	-	-	-	( $8.18 \times 10^{-9}$ ) $1.56 \times 10^{-8}$
			LgSm	-	-	( $8.18 \times 10^{-9}$ ) $1.01 \times 10^{-8}$	-
<b>Percent Decrease in Error</b>	NNE being used for predicting	Small Phytoplankton	PI Control	-	20.59%	-	-
			LgSm	38.20%	-	-	-
		Large Phytoplankton	PI Control	-	-	-	-90.87%
			LgSm	-	-	-23.11%	-

### 4.3 Case 3 – Different ESMs: Prognostic vs. Diagnostic Biological Equations, Identical Physical Circulations

520 From Cases 1 and 2, we [learned/learn](#) from our results that NNEs [were/are](#) capable of discerning differences in apparent relationships between model runs of the same ESM. For Case 3, we [wanted to](#) apply these principles to different ESMs to quantify the differences in the apparent relationships and highlight challenges that arise in comparing relationships between ESMs. The model runs of Cases 1 and 2 using BLING as a BC [afforded/affords](#) us the opportunity to test a

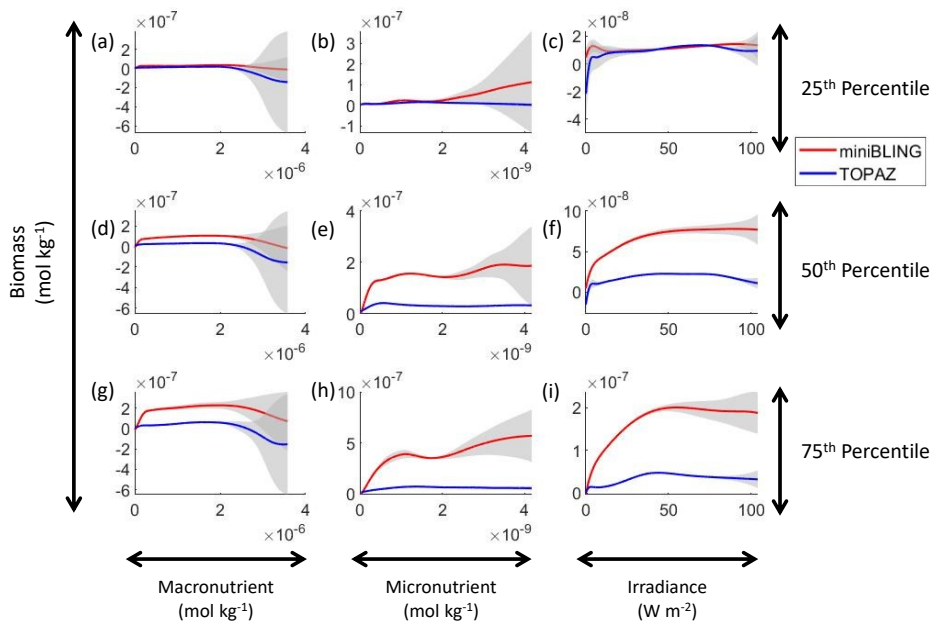


**Figure 11:** Sensitivity analysis plots for phytoplankton biomass for Case 3. Each line is the prediction for the NNE specific to each ESM and the color of each line represents the ESM (miniBLING—Red; TOPAZ—Blue). The gray region around each line shows one standard deviation in the predictions of the individual NNs that make up each NNE (ex. The gray region around the solid red curves shows the standard deviation in the predictions of the 25 NNs that make up that particular NNE). The rows correspond to the percentile value at which the other predictor variables were held constant (ex. Box (a) varies the macronutrient across its min-max range and holds the micronutrient and irradiance at their respective 25<sup>th</sup> percentile values). Columns show the x-axis variables as they vary between their min-max range. The y-axis in all subplots is the biomass concentration. Note that the biomass scale changes with each subplot.

525 “best-case” scenario for predicting biomass from nutrients and [light irradiance](#) because of the tight coupling of growth rate and biomass ([ie.i.e.](#), knowing the growth rate means we know the biomass). In Case 3, the ESMs have different biogeochemical codes ([ie.i.e.](#), different biological equations) and identical physical circulations. One ESM (ESM2Mo with miniBLING as BC, referred to as miniBLING) [was](#) comparable to the BLING formulation in that the growth rate [was](#) tightly coupled with the biomass. However, the other ESM (ESM2Mo with TOPAZ as BC, referred to as TOPAZ) [did](#) not have as tight of a coupling. The TOPAZ simulation [allowed](#) biomass to be advected and

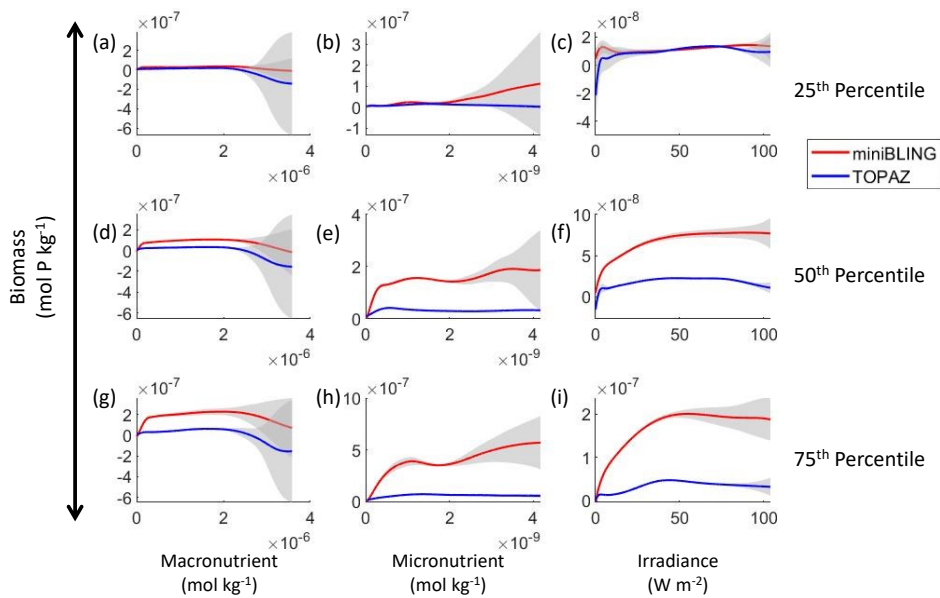


**Figure 11:** Sensitivity analysis plots for phytoplankton biomass for Case 3. Each line is the prediction for the NNE (i.e., the average prediction of 25 NNs) specific to each ESM and the color of each line represents the ESM (miniBLING – Red; TOPAZ – Blue). The gray region around each line shows one standard deviation in the predictions of the individual NNs that make up each NNE (e.g., the gray region around the solid red curves shows the standard deviation in the predictions of the 25 NNs that make up that particular NNE). The rows correspond to the percentile value at which the other predictor variables were held constant (e.g., box (a) varies the macronutrient across its min-max range and holds the micronutrient and irradiance at their respective 25<sup>th</sup> percentile values). Columns show the x-axis variables as they vary between their min-max range. The y-axis in all subplots is the biomass concentration. Note that the biomass scale changes with each subplot.

530 diffused in the same way as nutrients, effectively making biomass a function of nutrients and physical circulation, which is more typical of ESMs and likely true in the real ocean, as well.



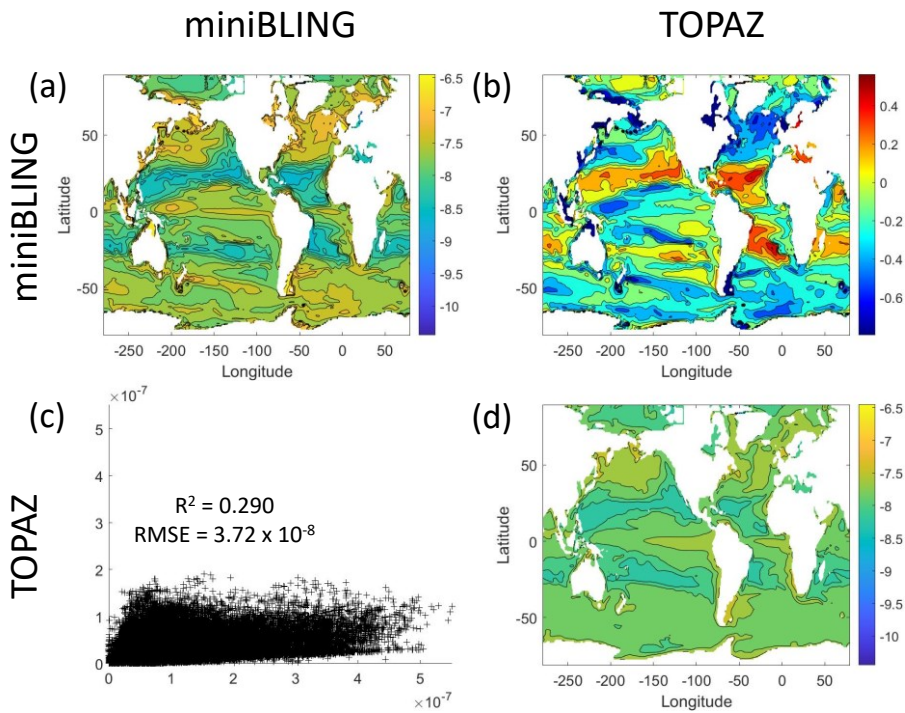


**Figure 12:** Comparison of the ESMs for total phytoplankton biomass in Case 3 in which circulation is given by ESM2Mo, but the the BCs are different. The units for biomass in all subplots are mol kg<sup>-1</sup>. The subplots show point-by-point scatter plots comparing the ESMs against one another (c), yearly averaged log10 biomass plots for each ESM (a and d), and the log10 relative ratios comparing the yearly averaged contour plots of the ESMs (b). The x-axis and y-axis of the scatter plots (c) correspond to the horizontal/vertical ESM labels, respectively (ex. Box (c) shows the miniBLING simulation on the x-axis and the TOPAZ simulation on the y-axis). The yearly averaged log10 contour plots (a and d) correspond to the matching horizontal/vertical ESM labels (ex. Box (a) shows the yearly averaged log10 biomass of miniBLING). The log10 relative ratios (b) were calculated as the ESM listed on the horizontal axis divided by the ESM listed on the vertical axis (ex. Box (b) shows TOPAZ divided by miniBLING).

Our results indicate that the phytoplankton in the two ESMs react differently to the same conditions. It should be noted that total phytoplankton biomass [was](#) used for Case 3, rather than splitting the biomass into large and small because phytoplankton output by the miniBLING BC is not differentiated into size classes. The sensitivity analysis shows that the miniBLING simulation produces higher biomass concentrations than the TOPAZ simulation under the same

535

**Table 5:** The performance metrics for the NNEs being used to predict the outcome of the other ESM of Case 3. In the top half of the table, the R-squared and RMSE are listed. The values in parentheses are the values from comparing the respective ESMs against one another (these are the same values listed in the respective scatter plot of Fig. 12). The values outside the parentheses are the values from using the trained NNE of the ESM listed in the row to predict the outcome of the ESM in the column (ex. The NNE trained on the TOPAZ simulation was used to predict the outcome of the miniBLING using the predictor values computed using the miniBLING simulation. These values were compared against the actual values of the miniBLING simulation to compute the RMSE of  $3.91 \times 10^{-8}$ ). In the bottom half of the table is the percent decrease in RMSE from the number listed inside the parentheses to the RMSE outside the parentheses (a negative percent means that the error increased).

				Case being predicted	
				miniBLING	TOPAZ
<b>R-squared</b>	NNE being used for predicting	miniBLING	-	(0.29)	0.3985
		TOPAZ	(0.29)	0.5405	-
<b>RMSE</b>	NNE being used for predicting	miniBLING	-	( $3.72 \times 10^{-8}$ )	$7.79 \times 10^{-8}$
		TOPAZ	( $3.72 \times 10^{-8}$ )	$3.91 \times 10^{-8}$	-
<b>Percent Decrease in Error</b>	NNE being used for predicting	miniBLING	-		-109.29%
		TOPAZ	-5.03%		-

conditions (Fig. 11), except at lower concentrations of nutrients where they seem to react similarly (Fig. 11 a, b, c). This is not entirely unexpected since the biomass values in the miniBLING simulation ~~were~~ generally much higher than those in the TOPAZ simulation, as can be seen in the point-by-point comparison (Fig. 12 c). However, not all of the biomass values in the miniBLING simulation ~~were~~ larger than those in the TOPAZ simulation. The subtropical Atlantic regions and northern subtropical Pacific ~~had~~ higher yearly averaged biomass values in the TOPAZ simulation compared to the miniBLING simulation (Fig. 12 a, b, d). As with Case 2, the additional test of asking the

540

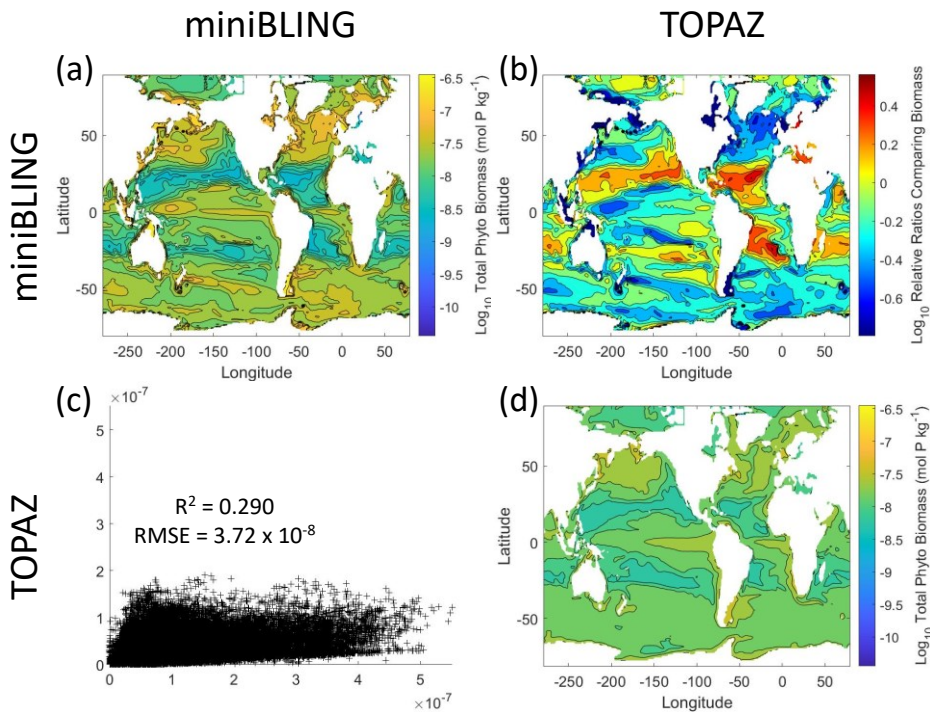


**Figure 12:** Comparison of the ESMs for total phytoplankton biomass in Case 3 in which circulation is given by ESM2Mo, but the BCs are different. The units for biomass in all subplots are mol P kg<sup>-1</sup>. The subplots show point-by-point scatter plots comparing the ESMs against one another (c), yearly averaged log<sub>10</sub> biomass plots for each ESM (a and d), and the log<sub>10</sub> relative ratios comparing the yearly averaged contour plots of the ESMs (b). The x-axis and y-axis of the scatter plots (c) correspond to the horizontal/vertical ESM labels, respectively (e.g., box (c) shows the miniBLING simulation on the x-axis and the TOPAZ simulation on the y-axis). The yearly averaged log<sub>10</sub> contour plots (a and d) correspond to the matching horizontal/vertical ESM labels (e.g., box (a) shows the yearly averaged log<sub>10</sub> biomass of miniBLING). The log<sub>10</sub> relative ratios (b) were calculated as the ESM listed on the horizontal axis divided by the ESM listed on the vertical axis (e.g., box (b) shows TOPAZ divided by miniBLING).

NNEs trained on the output of one ESM to predict the the output from the other ESM reinforcedreinforces the result that different apparent relationships wereare found from an increase in error for both ESMs (Table 5).

545

The challenge of comparing the results of different ESMs wasis evident in Case 3. For example, the performance metrics for the model runs in Cases 1 and 2 wereare relatively high in both the training and testing subsets, but the

**Table 5:** The performance metrics for the NNEs being used to predict the outcome of the other ESM of Case 3. In the top half of the table, the R-squared and RMSE are listed. The values in parentheses are the values from comparing the respective ESMs against one another (these are the same values listed in the respective scatter plot of Fig. 12). The values outside the parentheses are the values from using the trained NNE of the ESM listed in the row to predict the outcome of the ESM in the column (e.g., the NNE trained on the TOPAZ simulation was used to predict the outcome of the miniBLING using the predictor values computed using the miniBLING simulation. These values were compared against the actual values of the miniBLING simulation to compute the RMSE of  $3.91 \times 10^{-8}$ ). In the bottom half of the table is the percent decrease in RMSE from the number listed inside the parentheses to the RMSE outside the parentheses (a negative percent means that the error increased).

			Case being predicted	
			miniBLING	TOPAZ
<b>R-squared</b>	NNE being used for predicting	miniBLING	-	(0.29) 0.3985
		TOPAZ	(0.29) 0.5405	-
<b>RMSE</b>	NNE being used for predicting	miniBLING	-	( $3.72 \times 10^{-8}$ ) $7.79 \times 10^{-8}$
		TOPAZ	( $3.72 \times 10^{-8}$ ) $3.91 \times 10^{-8}$	-
<b>Percent Decrease in Error</b>	NNE being used for predicting	miniBLING	-	-109.29%
		TOPAZ	-5.03%	-

performance metrics for the TOPAZ simulation in Case 3 **were** much lower ( $R^2 > 0.97$  vs  $\sim 0.58$ , respectively; Table 2). **From these results alone, it is** unclear whether this drop in performance **was** because we **were** unable to characterize the TOPAZ simulation with NNEs using predictors common to both runs or whether we simply **did** not include enough relevant variables. To understand this, we **performed** a brief analysis in which we **trained** NNEs on specific variables and **measured** their performance with ESM output from CMIP5 ESM2M, which has TOPAZ as its BC (Table 6). One NNE **was** trained using only variables that directly affected the phytoplankton growth rate (biology), one **was** trained using only variables that **did not** directly affect the growth rate (physics), and another **was** trained with both sets of variables (all). Our results **indicated** that we **were** able to characterize ESM2M (and, by extension, results produced by using TOPAZ as a BC) with NNEs with the inclusion of more relevant variables, such as nitrate, ammonium, and silicate (RMSE  $\sim 5.90 \times 10^{-5}$  mol N  $m^{-3}$  [Table 6] vs. the average biomass value of  $3.14 \times 10^{-4}$  mol N  $m^{-3}$ ). Without the inclusion of all the relevant variables as predictors, the performance of the NNE trained on output from the TOPAZ simulation **suffered** compared to the NNE trained on the miniBLING simulation.

An additional challenge with comparing different ESMs is that certain variables may not be present in all ESMs. For example, one ESM may have phosphate included as a variable and another ESM may not. This presents a problem when using the sensitivity analyses, because each NNE needs to be presented with the same conditions for direct

**Table 6:** The performance metrics for the training and testing subsets of NNEs trained on different variable combinations of CMIP5 ESM2M output and details about the predictor/target variables.

Variable Groupings	Predictor Variables	Target Variable	Training Data		Testing Data	
			R-squared	RMSE	R-squared	RMSE
All Variables	1) Nitrate (mol m <sup>-3</sup> )	Phytoplankton Concentration (mol N m <sup>-3</sup> )	0.9756	3.61 x 10 <sup>5</sup>	0.9754	3.65 x 10 <sup>5</sup>
	2) Ammonium (mol m <sup>-3</sup> )					
	3) Phosphate (mol m <sup>-3</sup> )					
	4) Dissolved Iron (mol m <sup>-3</sup> )					
	5) Silicate (mol m <sup>-3</sup> )					
	6) Temperature (K)					
	7) Net Downward Shortwave Flux (W m <sup>-2</sup> )					
	8) Mixed Layer Thickness (m)					
	9) Surface X-Velocity (m s <sup>-1</sup> )					
	10) Surface Y-Velocity (m s <sup>-1</sup> )					
	11) Upward Ocean Mass Transport at 45 m Depth (kg s <sup>-1</sup> )					
Only Variables Directly Affecting Phytoplankton Growth Rate	1) Nitrate (mol m <sup>-3</sup> )	Phytoplankton Concentration (mol N m <sup>-3</sup> )	0.9358	5.87 x 10 <sup>5</sup>	0.9352	5.93 x 10 <sup>5</sup>
	2) Ammonium (mol m <sup>-3</sup> )					
	3) Phosphate (mol m <sup>-3</sup> )					
	4) Dissolved Iron (mol m <sup>-3</sup> )					
	5) Silicate (mol m <sup>-3</sup> )					
	6) Temperature (K)					
	7) Net Downward Shortwave Flux (W m <sup>-2</sup> )					
Only Variables NOT Directly Affecting Phytoplankton Growth Rate	1) Mixed Layer Thickness (m)	Phytoplankton Concentration (mol N m <sup>-3</sup> )	0.3268	1.90 x 10 <sup>4</sup>	0.3279	1.91 x 10 <sup>4</sup>
	2) Surface X-Velocity (m s <sup>-1</sup> )					
	3) Surface Y-Velocity (m s <sup>-1</sup> )					
	4) Upward Ocean Mass Transport at 45 m Depth (kg s <sup>-1</sup> )					

565 comparability. One potential method for mitigating this could be to use proxy-variables, such that variables not  
 570 common to both ESMs could be modified to represent the missing variables. For example, if one ESM ~~had~~has  
 phosphate as a variable, ~~and~~ another ESM ~~did~~does not, it might be possible to modify a variable that would be  
 equivalent to phosphate, such as nitrate. Using the Redfield ratio of 16:1 for the N:P ratio, the nitrate variable could  
 be divided by 16 and thus be considered a proxy variable for phosphate. This proxy phosphate variable could then be  
 used in training the NNE particular to ~~the~~ applicable ESM, so all NNEs would be trained using the same predictors.

**Table 6:** The performance metrics for the training and testing subsets of NNEs trained on different variable combinations of CMIP5-ESM2M output and details about the predictor/target variables.

Variable Groupings	Predictor Variables	Target Variable	Training Data		Testing Data	
			R-squared	RMSE	R-squared	RMSE
All Variables	1) Nitrate ( $\text{mol m}^{-3}$ )	Phytoplankton Concentration ( $\text{mol N m}^{-3}$ )	0.9756	$3.61 \times 10^5$	0.9754	$3.65 \times 10^5$
	2) Ammonium ( $\text{mol m}^{-3}$ )					
	3) Phosphate ( $\text{mol m}^{-3}$ )					
	4) Dissolved Iron ( $\text{mol m}^{-3}$ )					
	5) Silicate ( $\text{mol m}^{-3}$ )					
	6) Temperature (K)					
	7) Net Downward Shortwave Flux ( $\text{W m}^{-2}$ )					
	8) Mixed Layer Thickness (m)					
	9) Surface X-Velocity ( $\text{m s}^{-1}$ )					
	10) Surface Y-Velocity ( $\text{m s}^{-1}$ )					
	11) Upward Ocean Mass Transport at 45 m Depth ( $\text{kg s}^{-1}$ )					
Only Variables Directly Affecting Phytoplankton Growth Rate	1) Nitrate ( $\text{mol m}^{-3}$ )	Phytoplankton Concentration ( $\text{mol N m}^{-3}$ )	0.9358	$5.87 \times 10^5$	0.9352	$5.93 \times 10^5$
	2) Ammonium ( $\text{mol m}^{-3}$ )					
	3) Phosphate ( $\text{mol m}^{-3}$ )					
	4) Dissolved Iron ( $\text{mol m}^{-3}$ )					
	5) Silicate ( $\text{mol m}^{-3}$ )					
	6) Temperature (K)					
	7) Net Downward Shortwave Flux ( $\text{W m}^{-2}$ )					
Only Variables NOT Directly Affecting Phytoplankton Growth Rate	1) Mixed Layer Thickness (m)	Phytoplankton Concentration ( $\text{mol N m}^{-3}$ )	0.3268	$1.90 \times 10^4$	0.3279	$1.91 \times 10^4$
	2) Surface X-Velocity ( $\text{m s}^{-1}$ )					
	3) Surface Y-Velocity ( $\text{m s}^{-1}$ )					
	4) Upward Ocean Mass Transport at 45 m Depth ( $\text{kg s}^{-1}$ )					

## 5 Summary and Conclusions

A challenge of using ESMs is understanding why different ESMs yield different results, even when they are run under similar conditions. Our objective with this manuscript was to investigate the extent to which NNEs could characterize differences across ESMs through differences in circulation vs differences in biological formulations. We approached this objective by exploring three cases:

1. In the first case, we compared three configurations of an ESM that had identical intrinsic biological relationships but different physical circulations. The purpose of this case was to quantify the extent to which differences in physical circulations between model runs of the same ESM could affect the apparent relationships found by NNEs.
2. In the second case, we compared two model runs from the same ESM, except that the intrinsic biological equations were different, and the physical circulations were similar. The purpose of this case was to quantify the extent to which NNEs found differences in the apparent relationships and the size of those differences.
3. In the third case, we used two different ESMs that had different intrinsic biological relationships but identical physical circulations. The greatest difference between them was that in one ESM (ESM2Mo with TOPAZ as

585 BC), biomass was able to be advected and diffused making it a function of nutrients, ~~light~~irradiance, and  
circulation. This was in contrast to the other ESM (~~ESM2Mo~~ESM2M with miniBLING embedded as BC)  
where biomass was only a function of nutrients. The purpose of this case was to apply what we had learned in  
the first two cases to a more realistic ESM to quantify differences in the apparent relationships and identify any  
challenges.

590 Our results ~~indicate~~indicated that when all the relevant variables ~~are~~were included as predictors, the NNEs ~~are~~reserved  
as a parsimonious representation of the ESMs ~~and we can be relatively confident in their predictions. This confidence~~  
~~then allows us to query these NNEs using sensitivity analyses to find the apparent relationships, which provide~~  
~~information on the relationships between the predictor and target variables.~~

595 ~~With the first case, the similar performance metrics in the within and cross model comparison, along with the~~  
~~overlapping apparent relationships demonstrated that the~~and second cases, NNEs were able to attribute differences  
between the model runs to physics. ~~Likewise, in the second case, where the biological relationships differed, the NNEs~~  
~~were capable of attributing differences between the model runs to~~ and biological factors ~~and were able to identify the~~  
~~elements of that formulation that were different.~~

600 ~~With the~~ respectively. The third case, ~~we were able to show~~ demonstrated that ~~it is possible~~ NNEs could be used to  
compare ~~the~~ apparent relationships between ~~two~~ different ESMs and ~~that~~ find their key differences ~~can be found~~.  
~~However, this case also highlighted~~ along with highlighting some of the challenges ~~when comparing output from~~  
605 ~~multiple ESMs. In order to adequately capture the variability and achieve high performance metrics, all relevant~~  
~~variables for predicting an outcome must be included as predictors for each NNE. However, this presents a problem~~  
~~when one ESM may have a variable and another ESM does not. One possible solution is to use proxy variables, such~~  
~~that one variable can be modified to be representative of another.~~ in applying this to more realistic models.

610 The results of our study suggest that oceanographers and climate scientists could use the methods we have  
demonstrated to compare apparent relationships between ESMs, in addition to using spatiotemporal distributions and  
time series. This is not to say that spatiotemporal information is not important; rather, the relationships and  
spatiotemporal information can be used to inform one another. For example, in a side-by-side comparison of contour  
plots between biomass and nitrate concentrations, one might expect to see high biomass in high nitrate regions.  
615 However, if low biomass is observed in a high nitrate region, this would suggest that another factor (such as phosphate)  
is limiting phytoplankton growth. By visualizing the apparent relationships, one would be able to observe that  
phosphate has a strong limitation factor on the phytoplankton. This could then be verified with the spatial contour plot  
of phosphate against the original biomass and nitrate contour plots.

620 In addition to comparing relationships between ESMs, the methods presented here ~~will~~can allow for the comparison  
of relationships found in observational datasets to the relationships in ESMs. ~~This will allow~~ allowing for better tuning

of the models and more accurate representations of the natural world and what changes we might expect under climate change. ~~For example, if the apparent relationships from observations were to indicate increased biomass with increased CO<sub>2</sub> concentrations but current ESMs were predicting lower biomass, modelers would be able to update the ESMs with more accurate representations or finer tuning of the parameters. We will report on these potential applications in future work.~~ Our results here show the “best case” for comparing models with observations. The prevailing assumption is that environmental conditions set biomass and that ecological details do not matter; if two places have the same nutrients, irradiance, and mixing, they will have the same phytoplankton biomass. Our methods demonstrate that we can evaluate the extent to which such dynamics usually hold. In a follow-up paper, our preliminary results show that these methods can explain a large portion of the variance (60-80%) in two satellite-derived observational datasets, along with greater than 90% across a suite of CMIP6 ESMs.

625

630



## Appendix A

This appendix provides additional information about the datasets used in each of the three cases, along with information about how each dataset was randomly sampled.

635

The sizes of the datasets were as follows: 77,328 datapoints for each model run in Case 1, 77,328 datapoints for each model run in Case 2, and 577,332 datapoints for each model run in Case 3. Each dataset was split into training and testing subsets with 60% of the full dataset going to the training subset and 40% going to the testing subset. The training subset for each model run contained 46,397 datapoints in Case 1, 46,397 datapoints in Case 2, and 364,399 datapoints in Case 3. The testing subsets for each model run contained 30,932 datapoints in Case 1, 30,932 datapoints in Case 2, and 230,934 datapoints in Case 3.

640

The composition of the training and testing subsets were determined by random sampling, such that they randomly sampled the full dataset in both space and time. Specifically, the random number generator function for MATLAB, 2019b was set to "twister" and the seed was set as "123" for reproducibility. Each datapoint was either part of the training subset or the testing subset; no observations were part of both.

645

#### **Code and Data Availability**

##### 650 **Availability**

The Matlab scripts (MATLAB, 2019) for [processing the outputs of the ESM model runs](#), training the NNEs, and constructing the tables and figures, ~~along with the ESM outputs used for each case~~ are available in the [following Zenodo repository](#) ~~(~~<https://doi.org/10.5281/zenodo.4774438>~~)~~ (Holder et al., 2021).

##### **Data Availability**

655 [The output of the ESM model runs \(which serve as the input for training the NNEs\) for each case are available in the following Zenodo repository: <https://doi.org/10.5281/zenodo.4774438> \(Holder et al., 2021\).](#)

#### **Author contribution**

The conceptualization and ~~the~~ methodology of the research was developed by CH and AG. The coding scripts that configured the data for training, trained the NNEs, and produced the tables/figures were written by CH. The analysis  
660 and interpretation of the data was carried out by CH and AG. AG and MAP ran the ESMs that produced the model output for Cases 1 and 2. MAP coded the LgSm version of the BLING BC used in Case 2. The original draft of the manuscript was written by CH and AG, with edits, suggestions, and revisions provided by MAP.

#### **Competing Interests**

The authors declare that they have no conflicts of interest.

##### 665 **Financial Support**

This research was supported by the National Science Foundation (~~NSF~~) Division of Ocean Sciences (~~OCE~~) (Grant No. 1756568) ~~and~~, the Department of Energy (Grant No. DE-SC0019344) [and the National Oceanographic and Atmospheric Administration \(Grant No. NA21OAR4310256\)](#).

## References

- 670 Bahl, A., Gnanadesikan, A., and Pradal, M.-A. (2019). Variations in Ocean Deoxygenation Across Earth System Models: Isolating the Role of Parameterized Lateral Mixing. *Glob. Biogeochem. Cycles* 33, 703–724. doi:10.1029/2018GB006121.
- Bahl, A., Gnanadesikan, A., and Pradal, M.-A. S. (2020). Scaling Global Warming Impacts on Ocean Ecosystems: Lessons From a Suite of Earth System Models. *Front. Mar. Sci.* 7. doi:10.3389/fmars.2020.00698.
- 675 Bopp, L., Resplandy, L., Orr, J. C., Doney, S. C., Dunne, J. P., Gehlen, M., et al. (2013). Multiple stressors of ocean ecosystems in the 21st century: projections with CMIP5 models. *Biogeosciences* 10, 6225–6245. doi:10.5194/bg-10-6225-2013.
- Dunne, J. P., Armstrong, R. A., Gnanadesikan, A., and Sarmiento, J. L. (2005). Empirical and mechanistic models for the particle export ratio. *Glob. Biogeochem. Cycles* 19. doi:https://doi.org/10.1029/2004GB002390.
- 680 Dunne, J. P., John, J. G., Shevliakova, E., Stouffer, R. J., Krasting, J. P., Malyshev, S. L., et al. (2013). GFDL's ESM2 Global Coupled Climate-Carbon Earth System Models. Part II: Carbon System Formulation and Baseline Simulation Characteristics\*. *J. Clim.* 26, 2247–2267. doi:10.1175/JCLI-D-12-00150.1.
- Duteil, O., and Oschlies, A. (2011). Sensitivity of simulated extent and future evolution of marine suboxia to mixing intensity. *Geophys. Res. Lett.* 38. doi:https://doi.org/10.1029/2011GL046877.
- 685 Eppley, R. W. (1972). Temperature and phytoplankton growth in the sea. *Fish. Bull.* 70, 1063–1085.
- Galbraith, E. D., Dunne, J. P., Gnanadesikan, A., Slater, R. D., Sarmiento, J. L., Dufour, C. O., et al. (2015). Complex functionality with minimal computation: Promise and pitfalls of reduced-tracer ocean biogeochemistry models. *J. Adv. Model. Earth Syst.* 7, 2012–2028. doi:10.1002/2015MS000463.
- Galbraith, E. D., Gnanadesikan, A., Dunne, J. P., and Hiscock, M. R. (2010). Regional impacts of iron-light  
690 colimitation in a global biogeochemical model. *Biogeosciences* 7, 1043–1064. doi:https://doi.org/10.5194/bg-7-1043-2010.
- Geider, R. J., MacIntyre, H. L., and Kana, T. M. (1997). Dynamic model of phytoplankton growth and acclimation: responses of the balanced growth rate and the chlorophyll a: carbon ratio to light, nutrient-limitation and temperature. *Mar. Ecol. Prog. Ser.* 148, 187–200.
- 695 Gnanadesikan, A., Bianchi, D., and Pradal, M.-A. (2013). Critical role for mesoscale eddy diffusion in supplying oxygen to hypoxic ocean waters. *Geophys. Res. Lett.* 40, 5194–5198. doi:https://doi.org/10.1002/grl.50998.

Hansen, L. K., and Salamon, P. (1990). Neural network ensembles. *IEEE Trans. Pattern Anal. Mach. Intell.* 12, 993–1001. doi:10.1109/34.58871.

700 [Henson, S. A., Cael, B. B., Allen, S. R., and Dutkiewicz, S. \(2021\). Future phytoplankton diversity in a changing climate. \*Nat. Commun.\* 12, 5372. doi:10.1038/s41467-021-25699-w.](#)

Holder, C., and Gnanadesikan, A. (~~2021a~~2021). Can machine learning extract the mechanisms controlling phytoplankton growth from large-scale observations? – A proof-of-concept study. *Biogeosciences* 18, 1941–1970. doi:10.5194/bg-18-1941-2021.

705 Holder, C., Gnanadesikan, A., and Pradal, M.-A. (~~2021b~~2021). Dataset and scripts for manuscript “Using ~~neural~~  
~~network ensembles~~Neural Network Ensembles to ~~separate biogeochemical~~Separate Ocean Biogeochemical  
and ~~physical components~~Physical Drivers of Phytoplankton Biogeography in Earth System Models”.”  
Zenodo, <https://doi.org/10.5281/zenodo.4774438>.

710 Laufkötter, C., Vogt, M., Gruber, N., Aita-Noguchi, M., Aumont, O., Bopp, L., et al. (2015). Drivers and uncertainties of future global marine primary production in marine ecosystem models. *Biogeosciences* 12, 6955–6984. doi:<https://doi.org/10.5194/bg-12-6955-2015>.

Ledwell, J. R., Watson, A. J., and Law, C. S. (1998). Mixing of a tracer in the pycnocline. *J. Geophys. Res. Oceans* 103, 21499–21529. doi:<https://doi.org/10.1029/98JC01738>.

MATLAB version 9.7.0.1319299 (R2019b) Update 5 (2019). Natick, Massachusetts: The Mathworks, Inc.

715 Oeschlies, A. (2001). Model-derived estimates of new production: New results point towards lower values. *Deep Sea Res. Part II Top. Stud. Oceanogr.* 48, 2173–2197. doi:10.1016/S0967-0645(00)00184-3.

Pradal, M.-A., and Gnanadesikan, A. (2014). How does the Redi parameter for mesoscale mixing impact global climate in an Earth System Model? *J. Adv. Model. Earth Syst.* 6, 586–601. doi:<https://doi.org/10.1002/2013MS000273>.

720 Scardi, M. (1996). Artificial neural networks as empirical models for estimating phytoplankton production. *Mar. Ecol. Prog. Ser.* 139, 289–299.

Schmidhuber, J. (2015). Deep learning in neural networks: An overview. *Neural Netw.* 61, 85–117. doi:10.1016/j.neunet.2014.09.003.

Formatted: Bibliography, Indent: Left: 0", First line: 0"

[Sweeney, C., Gnanadesikan, A., Griffies, S. M., Harrison, M. J., Rosati, A. J., and Samuels, B. L. \(2005\). Impacts of Shortwave Penetration Depth on Large-Scale Ocean Circulation and Heat Transport. \*J. Phys. Oceanogr.\* 35, 1103–1119. doi:10.1175/JPO2740.1.](#)

Tyrrell, T. (1999). The relative influences of nitrogen and phosphorus on oceanic primary production. *Nature* 400, 525–531. doi:10.1038/22941.